DEPARTMENT OF BIOCHEMISTRY
All India Institute of Medical Sciences
New Delhi- 110029

To,
The Sun Pharma
Science Foundation
India

31th August 2023

Subject: Application for sponsoring the nomination for Sun Pharma Science Scholars Awards-2023

Respected Members,

This is to inform you that I Ashu, PhD student under the supervision of Prof. Alpana Sharma in the Department of Biochemistry, AIIMS, New Delhi. I am applying for Sun Pharma Science Scholar award under the category of Biomedical research. Please find the detailed copy of the required documents for this application.

Kindly consider my application for the nomination.

Thanks and Regards,

Ashu
PhD student
Department of Biochemistry,
AIIMS, New Delhi-29

Title: Elucidating the role of memory T cells in Renal cell Carcinoma Patients.

Introduction:

According to the GLOBOCAN Cancer consortium (2021), there is an annual increment of 2% of new cases of Renal cell carcinoma (RCC) worldwide [1]. Till date, cytoreductive nephrectomy (CN) is still considered a gold standard procedure to treat advanced RCC [2]. The CARMENA (The Cancer du Rein Metastatique Nephrectomie et Antiangiogéniques (2018)) and SURTIME (Immediate Surgery or Surgery After Sunitinib Malate in Treating Patients With Metastatic Kidney Cancer (2017)) phase III and phase II respective clinical trials are a proof of it and also support nephrectomy for advanced RCC patients [3][4]. Nonetheless, surgery increases the comorbidities such as chronic kidney disease, hypertension, and morbid cardiac events which elevates the mortality rate in patients [5][6][7]. Additions of surgery, target-specific inhibitors for VEGF/PDGFR/mTOR pathway, have been utilized to increase disease-free survival in metastatic renal cell carcinoma [8]. However, these therapies are often inadequate and can lead to recurrence or progression of the cancer [6][5][9][7]. Recent studies conducted by the mRCC database consortium showed that the overall response rates (ORR) of checkpoint inhibitor therapies such as PD-L1 inhibitor (nivolumab) alone or in combination with VEGF inhibitor were between 31% to 40% in patients. Similarly, ORR for second-line, third- line, and fourth-line treatments were reportedly 22%, 24%, and 19%, respectively [10][11][12][13], and despite the promising efficacy of these treatments, further research is needed to improve existing outcomes. ORR of checkpoint inhibitors therapies have not been met from the first line to fourth line of treatment in mRCC, indicating the current treatment regimen for RCC is inadequate in providing long-term durable response. Therefore, developing a therapeutic strategy with an effective, efficient and long-term immune response within the tumor microenvironment is warranted.

$CD8^+$ memory T cells play a critical role in the body's immune response to pathogens and tumors, possessing properties of long-term maintenance and survival with involvement in antigenic stimulation, thereby maintaining immune memory [14]. However, $CD8^+$ memory T cells may become dysfunctional and lose their anti-tumor potential [15][16][17]. Understanding the mechanisms behind the maintenance and deterioration of $CD8^+$ memory T cells is critical for developing strategies to harness their full potential in fighting renal cancer. Potassium channel modulatory protein (KCMF1), a zinc finger protein, aids in regulating the turnover of misfolding protein aggregates and cellular organelles through the ubiquitination pathway under stressful conditions. KCMF1 protein interacts with Ubiquitin-conjugating enzyme E2 A (UBE2A/RAD6) and Ubiquitin Protein Ligase E3 Component N-Recognin 4 (UBR4) at the C- and N-terminal domains respectively, forming a ubiquitin ligase E2-E3 complex. The unique E2-E3 complex with a RING domain can reprogram the ubiquitin code of the destabilized proteins, redirecting them towards lysosomes for efficient degradation via autophagy instead of relying on UPS (Ubiquitin

Proteasome system) [18][19]. The potential contribution of this complex in regulation of autophagy in $CD8^+$ memory T cells in RCC currently remains unexplored.

2. Objectives:

1. **To phenotypically characterize the memory T cells subsets aiding in immune escape.**
2. **To elucidate the potent mechanisms and signaling molecules responsible for immune escape of T cells in RCC.**

3. Material and methods:

3.1 Sample collection: 30 ccRCC (clear cell renal cell carcinoma) cases and 30 controls were enrolled to investigate the underlying mechanisms. Blood samples from the patients and controls were collected after histopathological confirmation from the Urology Department, AIIMS, New Delhi. Tumor and adjacent non-tumor tissue biopsies were also collected from radical nephrectomy patients. The study was conducted after receiving ethical clearance from AIIMS Ethics Committee, and patients were carefully selected based on certain exclusion criteria. Written informed consent was obtained from all participants before their inclusion in the study.

3.2 Sample processing: Sample with 10 ml blood was processed for PBMCs separation using the Ficoll gradient method. Additionally, tumor tissue and adjacent non-tumor tissue from the patients were obtained by urology surgeons and stored in the tissue storage solution from Milteny. Within 24 hours of sample collection, both blood and tissue samples were prepared for processing and sorting.

3.3 Phenotypic characterization of CD8+ memory T cells subsets: 1.5×106 cells/ml were aliquoted, incubated with titrated flourochrome alongside the conjugated antibodies for markers: CD8-PerCpCy5.5 (Catalogue no-45-0088-42 ;; clone-RPA-T8), CD4- BV421 (Catalogue no-62-0047-42 ;; clone- SK3(SK-3), CCR7-BV605 (Catalogue no-63- 1979-42 ;; clone- 3D12), CD45RA-FITC (Catalogue no-555488 ;; clone-32877), CD45RO-PE (Catalogue no- 20-24-827 ;; clone-UCHL1), CD107a-PE-Cy5 (Catalogue no-20-87-212 ;; clone- ebioH4A3) and CD25-APC-Cy7 (Catalogue no-21-61-984 ;; clone- BC96) from BD Biosciences, USA. For intracellular staining of FOXP3-PE (Catalogue no-56-00-46 ;; clone- 259D/C7 ;; BD pharminogen) transcription factor, surface-stained cells were fixed and permeabilized using BD Fixation buffer (BD Cytofix/Cytoperm; Catalogue no; 51-2090KZ) and Permeabilzation buffer (BD Perm/wash; Catalogue no-51-2091KZ) from (BD Biosciences, San Diego, USA). After fixation, samples were incubated with FOXP3-PE antibody in permeabilization buffer overnight. Before staining, dead cells were removed using Zombie dye-Indo-I. Subsequently, the cells were washed and transferred into the FACS tube. During acquisition, one million CD8+ T cells were registered in each tube on

BD LSRFortessa™ Cell Analyzer machine (BD, USA). The data were analyzed using Tree Star FlowJo X 10.0.7 software. For CD8+ memory T cells identification including their activation and regulatory markers, we created two panels (Panel-1 for activated memory T cells * CD4, CD8, CD45RA, CCR7, CD107a, CD45RO and Panel-2 for regulatory memory T cells * CD4, CD8, CD45RA, CCR7, CD25, FOXP3); details of panels were enclosed in the supplementary data file. From live cells, CD4+ and CD8+ T cells were gated from live cells and further sub gated for CD8+ memory T cells subsets central memory T cells (TCM ;; CD45RA-CCR7+); effector memory T cells (TEM ;; CD45RA-CCR7-); effector T cells (TEFF ;; CD45RA+CCR7-) and naïve cells (CD45RA+CCR7+). Further, each subset was gated for degranulation marker CD107a and regulatory marker FOXP3+CD25+. Gating strategy was represented in supplementary file.

3.4 Tissue sample processing: 20g tissues were chopped into pieces and incubated into 10ml dissociation buffer ((Hank's buffer without Ca2+ and Mg2+, (collagenase type IV 2mg/ml), DNase I (100 µg/ml)) and stirred for 30 min at 37 °C. Samples were pipetted and vortexed every 10 minutes during the incubation. Cell suspensions were passed through a 70-100µm cell strainer, to collect and store the supernatant. Collected single cells were washed using Hank's buffer containing 50mM EDTA and then were preceded for sorting.

3.5 Sorting of CD8 memory T cells: 1x106 cells/ml from study participants were used for CD8+ memory T cells sorting using EasySepTM Human memory CD8+ T cells Enrichment MACS isolation Kit from STEM CELLS Technologies (Catalogue no-19159 ;; clone-100015452) as per manufacturer's instructions. Cells were stained for antibodies of other cells type such as leukocytes, lymphocytes, neutrophils, thereby negatively selecting out CD8+ memory T cells. Thereafter, cells were harvested and aliquoted into multiple eppendorf to perform Real time-PCR, Annexin/PI, JC.1 and confocal staining. Subsequently, negatively selected CD8+ memory T cells were stained for CD8-PerCPCy5.5, CD45RO-PE antibodies, rendering a confirmation of 90% purity of CD8+ memory T cells by flow cytometry.

3.6 JC.1 staining: To estimate mitochondrial membrane depolarization, CD8+ memory T cells were stained and incubated with 2µM of JC1 dye solution (Catalogue no. T4069 ;; CAS no. 3520-43-2, Sigma Aldrich) for 30 minutes at 37˚C in dark. Later, red/green signal of stained cells were analyzed by flow cytometry.

3.7 Annexin/PI staining: CD8+ memory T cells were incubated with 100µl of Annexin V binding buffer, 4µl Annexin-V-FITC dye and 8µl PI (FITC Annexin V Apoptosis Detection Kit with PI, Catalogue no. 640914, Bio legend, USA) for 20 minutes at room temperature. Finally, data were analyzed using Tree Star FlowJo X 10.0.7 software.

3.8 Confocal staining of sorted CD8+ memory T cells from PBMCs and TRMs (Tissue resident CD8+ memory T cells): 1x105 cells/ml sorted cells were poured into Poly-L-Lysine coating coverslip and incubated for 30 min for adherence. Cells were then incubated with 100% chilled methanol for 7 min at -20°C. After washing, non-specific sites on cells were blocked using blocking buffer (1%BSA, 0.5% tritonX-100 in 1X PBS). Primary antibody against ubiquitin and autophagy markers were added; anti-rabbit KCMF1 (Dilution 1: 100 ;; Catalogue no-PA5-40623 ;; clone-UF279271), anti-mouse UBR4 (Dilution 1: 200 ;; Catalogue no-sc-100615 ;; clone-J0919), anti-rabbit RAD6 (Dilution 1: 100 ;; Catalogue no- ab155001;; clone-GR2780462), anti-mouse KCMF1(Dilution 1:100 ;; Catalogue no-sc- 390051 ;; clone- A-3), anti-mouse LC3B (Dilution 1: 200 ;; Catalogue no-sc271625 ;; clone- CC318), anti-mouse P62 (Dilution 1: 200 ;; Catalogue no-sc-166870 ;; clone-G-8) from (Thermo scientific-USA, SANTA CRUZ- Biotechnology, USA). For tissue, 4mm formalin fixed tumor and non-tumor tissue sections were sliced using microtome and placed onto poly- lysine coated slides. The sample was treated with a series of xylene and ethanol gradient. Then, antigens were retrieved using tri-sodium citrate buffer pH-6 (Merck, USA) via heat-antigen retrieval method. Non-specific binding sites were blocked using 5% BSA plus Triton X-100 for 1h at RT. Subsequently, sections were incubated with primary antibody against autophagy LC3B and p62 consecutively with integrin protein CD103 (anti-hamster CD103: Catalogue no. ab25198 ;; clone-GR3390927) from (Thermo scientific-USA). The next day, anti-hamster: Alexa Fluor 647 (Catalogue no- ab-25198 ;; clone-2E7 from Invitrogen Thermo Scientific, USA), anti-mouse: DyLight™ 488 conjugate (Invitrogen Thermo Scientific, USA) and anti- rabbit: DyLight™ 550 conjugate (Invitrogen Thermo Scientific, USA) secondary antibodies were used to tag primary antibodies. Lastly, Fluoroshield TM with 4′,6-diamidino-2-phenylindole (DAPI) mounting media (Catalogue no: F6057;; clone SLCG8078 ;; SIGMA-USA) were used to stain nucleus and mount the slide. The mounting media with DAPI occasionally presents a “glaring effect” with blue background noise. This was avoided by ensuring that the cover glass is tightly mounted on the glass slide (light weights can be placed on the cover glass to ensure mounting media is evenly distributed with no air bubbles) and the imaging tissue section is flat. Scanned and Z- stack images were captured on confocal microscope (LSM 980; Carl Zeiss, Germany) at 100X for sorted cells from blood and 63X for tissue.

3.9 Image analysis: Laser scanning confocal microscope (LSM 980; Carl Zeiss, Germany) were used for image capturing. All the fluorescence images were captured under the same settings for every experimental set. Images were captured using a plan apochromatic 63X,0.95 NA objectives for tissue sections or a plan apochromatic 100X, 1.4 NA objectives for sorted cells from blood. The following lasers were used for exciting the samples: (i) 30 mW 405 nm diode laser at 0.2% – 4% power. (ii) 35 mW 488 nm argon-multiline laser at 3% – 12% power. (iii) 20 mW 561 nm diode-pumped solid state (DPSS) laser at 5% power. (iv) 2 mW 633 nm He-Ne laser at 10% – 12% power.

The pinhole was set to 1 Airy Unit and master gain, digital offset and digital gain were set to 650V, 24 and 1.0, respectively for all cases. All images were captured at 1.0X zoom. Colocalization analyses were done using ZEN3.1 software (Carl Zeiss, Germany). The scatter plots and tables including Pearson's coefficient values were extracted from ZEN3.1 and compiled together. Fluorescence intensity values were calculated using ImageJ/Fiji software (National Institutes of Health, Bethesda, USA). Briefly, the freehand selection tool was used to select a DAPI-positive area in Fiji and the fluorescence intensity pixels corresponding to that area was measured. The fluorescence intensity was normalized to the DAPI area to account for any variability in the nuclear size. The images and graphs were compiled using Adobe Photoshop 7.0 software.

3.10 cDNA preparation and Real-time PCR: Blood and tissue sorted CD8+ memory T cells were stored in Trizol at -80ºC. RNA was isolated as per TRIZOL method and Integrity-quantity of RNA was checked using Nanodrop Spectrophotometer (Thermo, USA). The isolated RNA was used to synthesize complementary DNA (cDNA) using MuLV Reverse Transcriptase (Fermentas,USA). cDNA was used as a template for real-time PCR (BioRad, USA) using primers specific to the different molecules. Maxima SYBR Green qPCR Master Mix (2X) (Fermentas, USA) was used to perform the relative expression analysis of KCMF1, LC3B, P62. The data were normalized to housekeeping gene GAPDH and expressed as 2-ΔCt.

3.11 microRNA specific cDNA preparation: After RNA isolation and quantification, miRNA specific cDNA were prepared using miScript II RT Kit (Qiagen, Germany) as per kit protocol. Total RNA containing miRNA were used as template for reverse transcription by miScript Reverse Transcriptase Mix, Nucleic Mix and 5x miScript HiFlex Buffer to convert all RNA species into cDNA. Thereafter, the samples were diluted 1:10 times using nuclease free water. Diluted cDNA were further used to amplify miRNA 210 and SnoRD as housekeeping using Maxima SYBR Green qPCR Master Mix at slow ramp rate (2X) (Fermentas, USA) in real-time PCR machine (BioRad, USA). Data were normalized and expressed as 2-ΔCt.

3.12 Preparation of standards and reagents for Inductively coupled plasma mass spectrometry (ICP-MS)

Minerals like Calcium (Ca), Potassium (K), Magnesium (Mg), Sodium (Na), and trace elements like Zinc (Zn), Iron (Fe), Copper (Cu), Selenium (Se), and Manganese (Mn) were analysed using Inductively coupled plasma mass spectrometry (ICP-MS) (NexION 2000, PerkinElmer). Standards were of analytical grade provided by PerkinElmer of concentration (1000 parts per million) for K, Mg, Ca, Fe, Cu, Se, Mn, and Zn. Working stock was prepared from solution having a concentration of 1ppm for Zn, Cu, Fe, Se, Mn and 100 ppm for K, Mg and Ca. Further standards prepared for analysis were 0.5, 1, 1.5, 2, 5, 10 and 20 parts per billion (ppb) K, Mg, Ca, Fe, Cu,Se, Mn and Zn whereas 0.5, 1, 1.5, and 2 ppm for K, Mg and Ca. Filtered through 0.2 micron filter, mili-Q water

18.2 Ω was used for preparation of standards. 1% nitric acid was prepared freshly by milli-Q stored in Tarson plastic bottles.

3.13 ICP-MS

First, the tumor (n=20) and non-tumor tissue sample (n=20) were powered using liquid nitrogen and sonicated at 50Amp for three times in RIPA lysis buffer to prepare the cell lysate. Obtained lysate were thawed and brought to room temperature. 50µl of cell lysate was taken and diluted to 5 ml (100 times) with 1% supra-pure nitric acid. After mixing the sample, it was centrifuged at 10,000 g for 15 min at room temperature. To prevent instrument clogging and interference from suspended particles, the sample was filtered with a 0.2-micron syringe filter before being injected into the nebulizer with the aid of a peristaltic pump.

3.14 Data analysis: Statistical analyses were performed in Prism (Graph-Pad Software, version 8.0e). FCS 3.1 data files were analyzed using Tree Star FlowJo X 10.0.7 software under same compensation matrix. For group analysis, Bonferroni-Dunn post hoc (Two-way ANOVA) test were used for unpaired non-parametric multiple comparisons of memory T cell subsets between patients and controls. Statistical significance of memory T cell subsets was determined with alpha = 0.05. Each row was analyzed individually, without assuming a consistent SD. To compare single variable between patients and controls, non-parametric Mann–Whitney U test were used to evaluate significance of real-time PCR, confocal and flow data sets. Data was demonstrated as Mean±SD amongst study participants. Real time data were expressed as 2-ΔCt where GAPDH and SnoRD were used as housekeeping to normalize the data.

Chapter -1

Evaluation of KCMF1 linked ubiquitin ligase and ion channels in tumor tissue samples

RESULTS:

1. Degradation of KCMF1 (E3) and its associated ubiquitin (E2) proteins (RAD6 and UBR4) in tumour tissue.

Transcriptional expression of KCMF1 was diminished in both PBMCs and tumor tissue from RCC patients when compared to adjacent non-tumor tissue (Fig.1a). Moreover, the expressions of E2-E3 proteins (KCMF1-UBR4-RAD6) were reduced in tumor tissue. The formation of punctate structures by KCMF1, RAD6, and UBR4 proteins in non-tumour tissue was clearly observable but absent in tumour tissue, indicating the potential disintegration and/or diffusion of the KCMF1, RAD6, and UBR4 protein complex in RCC tumour tissue (Fig.1b). Additionally, the structural integrity of the nuclear membrane was found to be altered in the tumor tissue of patients. These findings suggest that there is a disturbance in the native structure of E2-E3 complex domains a its localization in RCC patients.

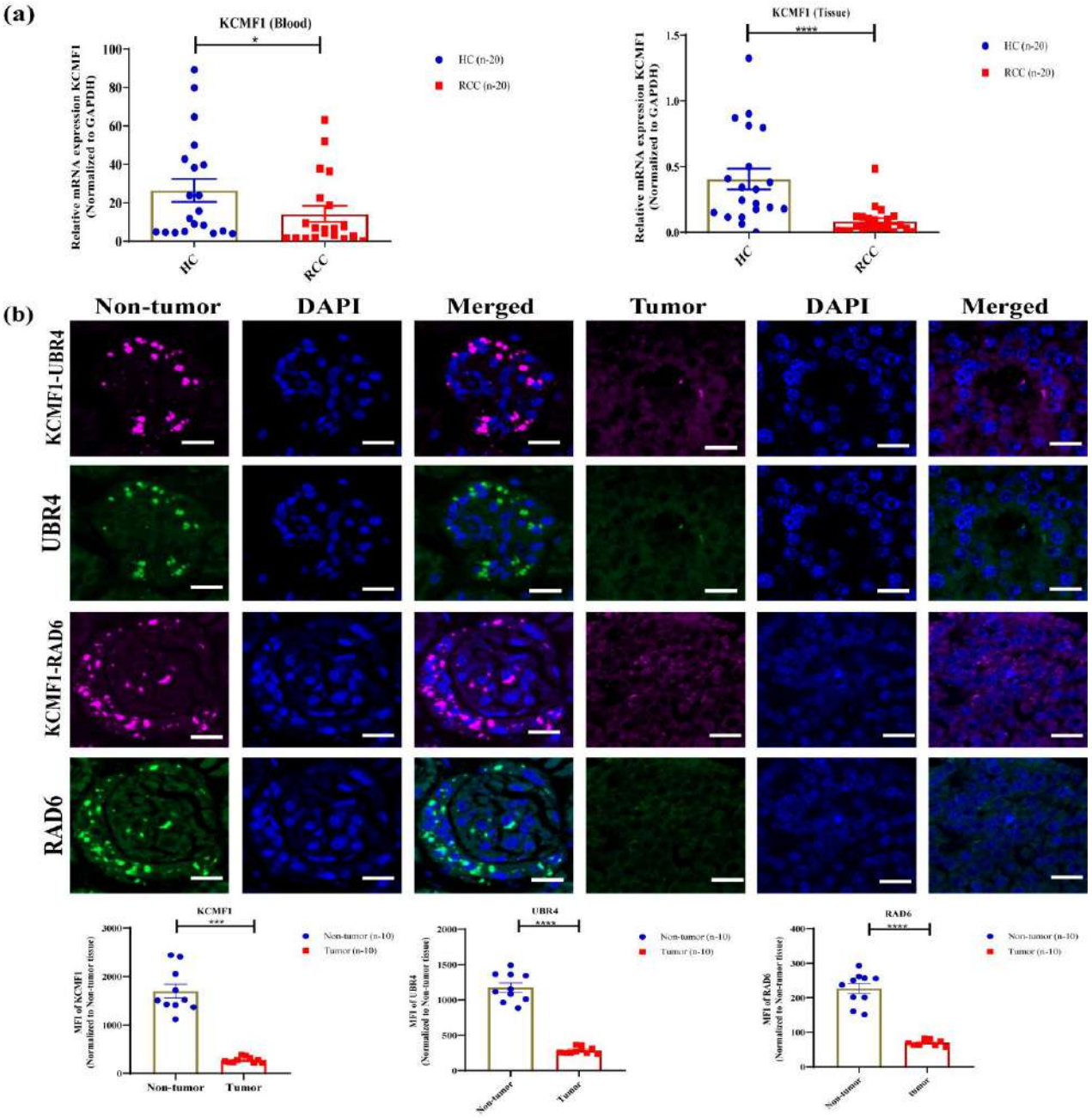

Figure 1: Quantification of KCMF1 and its associated proteins (UBR4 and RAD6) in tumor and non-tumor tissue. (a). The expression of KCMF1 in PBMCs (n=20) and tissue (n=20) was represented using a bar graph. (b). Dual immunostaining of KCMF1-UBR4 and KCMF1-UBR4 in non-tumor and tumor tissue (n=10) was visualized through representative confocal images. Scale bars (20um) were shown in the images. The quantification of KCMF1, RAD6, and UBR4 in study subjects (n=10) is presented in the respective image panel. Statistical significance was denoted as *p<0.05, ***p<0.001, ****p<0.0001.

2. Diminished constitution of E2-E3 (RAD6-KCMF1-UBR4) ubiquitin ligase and its association with HIF1A target protein in tumor cells.

The formation of the E2-E3 complex is essential for the functioning of KCMF1 as a ubiquitin ligase protein [18]. Therefore, we conducted a measurement of the co-localization of the E2-E3

complex in tumor and non-tumor tissues using the Pearson correlation coefficient algorithm of MIP (maximum intensity projection) images in confocal microscopy. Our findings indicate that the domains of KCMF1-RAD6 and KCMF1-UBR4 proteins are reduced in tumor tissue, while in non-tumor tissue; each domain of the E2-E3 proteins remains intact **(Fig. 2a).** This suggests that the physical interaction between KCMF1 and RAD6, as well as UBR4, is absent in tumor cells, thereby affecting the formation of the ubiquitin ligase complex in RCC patients. Previous studies have demonstrated elevated expression of the HIF1α protein in RCC tumors due to the defective function of the vHL ubiquitin ligase [20]. Hence, we examined the expression of HIF1A in tumor tissues from the same patients we analyzed for KCMF1 expression. Our observations reveal an increased localization of activated HIF1A in the nucleus of tumor tissue compared to non-tumor adjacent tissue **(Fig. 2b).** These findings suggest that the defective KCMF1-associated ubiquitin protein complex may be accountable for the accumulation of HIF1A, in addition to the vHL ubiquitin complex, in the tumor tissue of RCC patients.

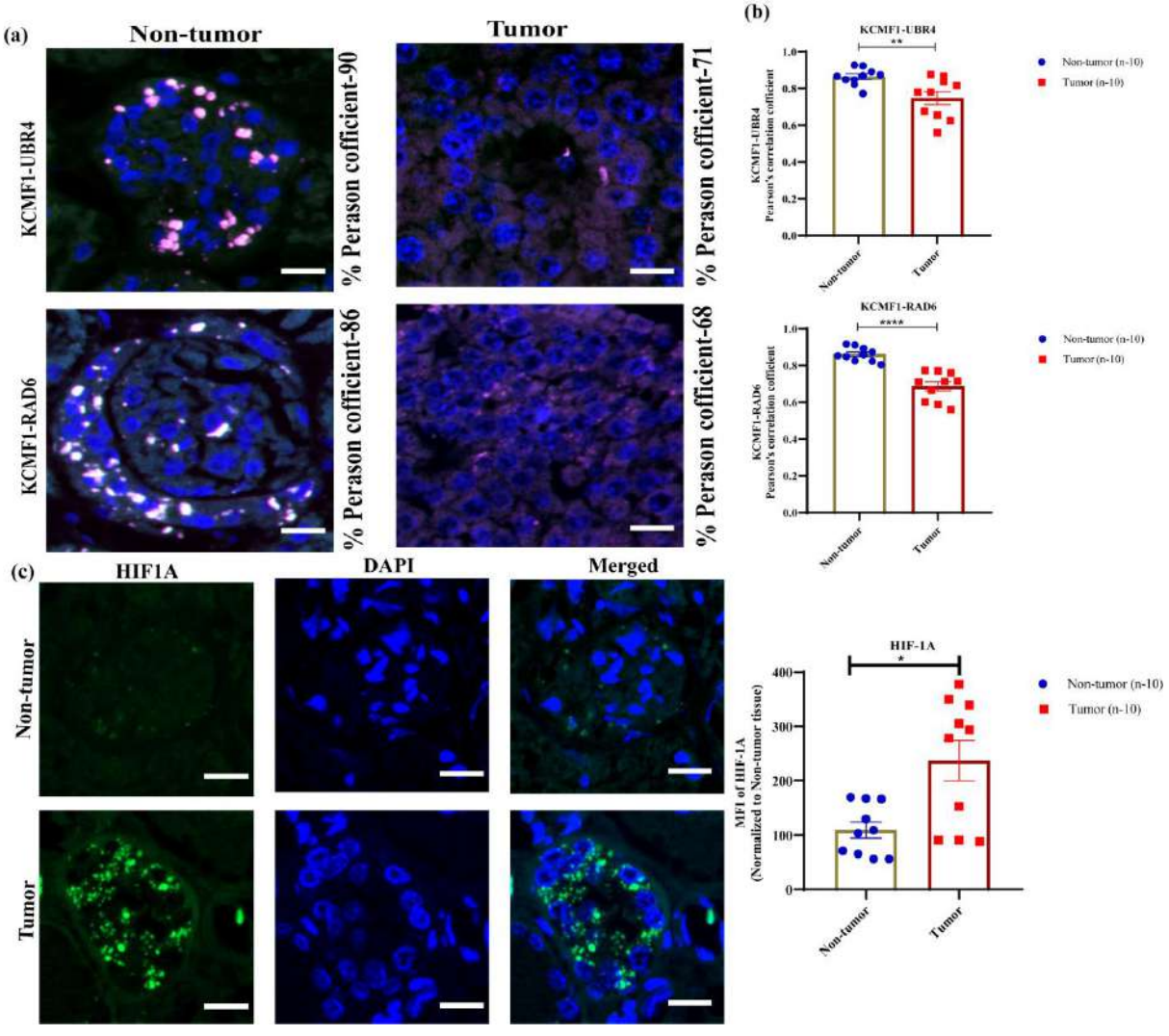

Figure 2: Detection of co-localization of RAD6-KCMF1-UBR4 ubiquitin ligase and HIF1A in study subjects. (a). The domains of KCMF1-UBR4 (upper panel) and KCMF1-RAD6 (lower panel) co-localization in non-tumor sample were completely abolished in tumor tissue (n=10). (b).

The amount of signal overlap between KCMF1-UBR4 and KCMF1-RAD6 in tumor and non-tumor tissue was quantified. (c). The expression of HIF1A (green color) was observed in tumor tissue (lower panel) and absent in non-tumor tissue (upper panel) (n=10). The quantification of HIF1A is shown in the adjacent graph (n=10). The scale bar (20um) is shown in the images. *p<0.05, **p<0.01, ****p<0.0001.

3. Reduction of autophagosome formation and substrate degradation *via* N-recognin p62 in tumor tissue.

KCMF1-induced E2-E3 protein complex triggers the degradation and autophagy processes in lysosomes [10]. A defect in the formation of the ubiquitin ligase could result in a malfunction in autophagy. Consequently, we examined the expression of autophagy-related proteins in RCC tumor tissue. Remarkably, we found a decrease in the transcription of LC3B and p62 in tumor tissue, while patients' PBMCs exhibited a significant increase in p62 gene expression (Fig. 3a). Similar to the KCMF1 protein complex, the punctate localization of LC3B and p62 proteins was only observed in non-tumor tissue (Fig. 3b). These findings suggest that the synthesis of autophagosome and cargo proteins, responsible for carrying ubiquitin-binding proteins for degradation, is impaired in the tumor tissue of RCC patients.

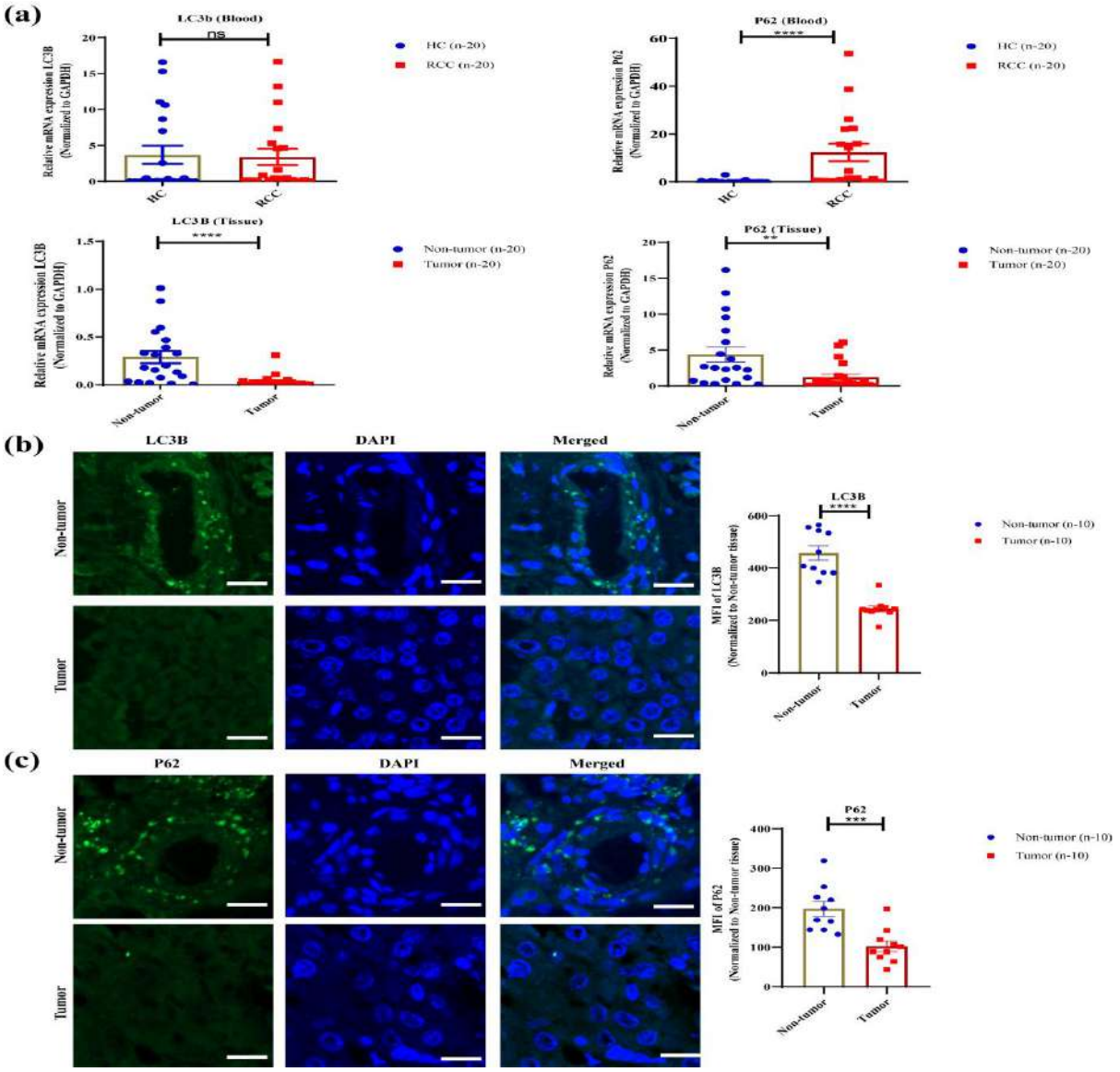

Figure 3: Analysis of autophagy in RCC tumor tissue. (a). The mRNA expression of LC3B and p62 in PBMCs (n=20) and tumor tissue (n=20) is represented by the bar diagram. The immunostained images demonstrate the presence of LC3B (green colour) punctate dots and p62 (green color) punctate dots in the non-tumor tissue and tumor tissue. The bar graph illustrates the MFI of LC3B and p62 in the study groups. The images contain a scale bar indicating a measurement of 20um. Statistical significance is indicated as **p<0.01, ***p<0.001, ****p<0.0001.

4. Alteration in ions concentration and ion channels in tumor tissue of RCC patients.

KCMF1, a potassium channel modulatory protein, plays a role in regulating the activity of potassium ion channels [21]. This zinc finger protein contains motifs that coordinate with two Zn ions for ligand binding and protein scaffolding. Currently, the exact mechanism by which KCMF1 regulates ion channel function remains largely unknown. To shed light on this, we investigated the concentration of essential ions, such as zinc, involved in their function. In RCC, we observed a decrease in zinc ion levels in tumor cells compared to non-tumor cells (Fig.4 (a)). However,

potassium and sodium concentrations were significantly elevated in tumor cells compared to non-tumor cells (Fig.4 (a)). These findings indicate that KCMF1 not only affects ubiquitination but also alters ion regulation. Furthermore, the expression of voltage-gated potassium channel (KV1.3) and calcium-dependent potassium channel (KCNN4) proteins were also found to be altered in tumor tissue compared to adjacent non-tumor tissue (Fig. 4 (b) (c)). Although western blot data reported increased expression of KCNN4 in RCC, confocal microscopy of tissue samples revealed a diffuse expression in tumor tissue and a punctuate expression in non-tumor tissue. This suggests that although KCNN4 may be higher in tumor tissue, its protein integrity is disturbed. Collectively, these pieces of evidence clearly indicate that KCMF1 becomes dysfunctional in tumor tissue.

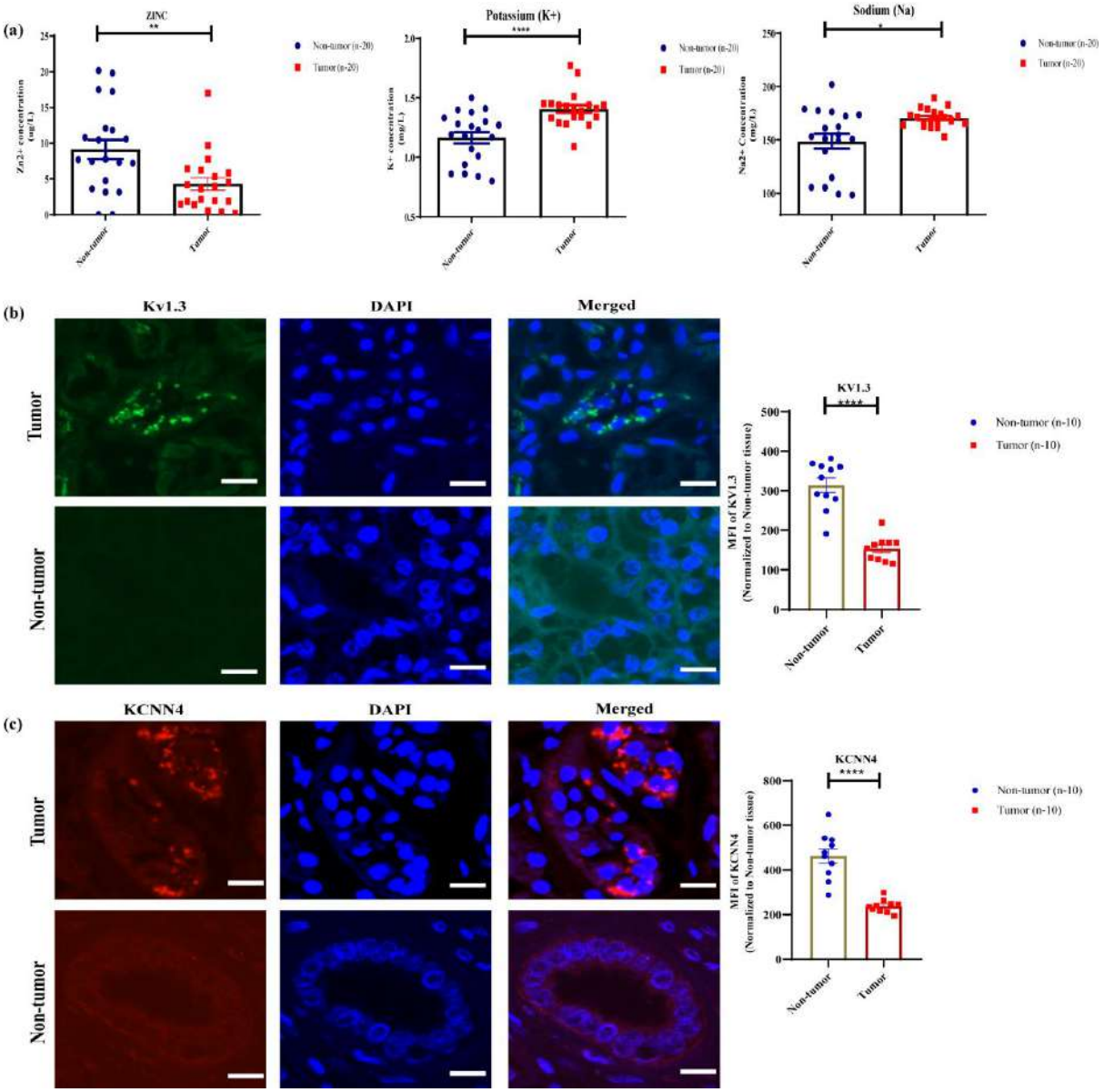

Figure 4: Detection of ions concentrations and ions channels in RCC tumor and non-tumor tissue. (a). Zinc, potassium, and sodium concentration were measured using ICP-MS (n=20) in both tumor and non-tumor tissue. Positive staining for the proteins KV1.3 (green, b) and KCNN4 (red punctate, c) was observed. The MFI of each protein was observed to be lower in the tumor tissue of RCC patients (n=10). The data was represented using a bar diagram with individual values

depicted as Mean±SEM. Scale bars (20um) were included in the images. Statistical significance was indicated as *p<0.05, **p<0.01, ****p<0.0001.

Discussion:

Our current findings discover new therapeutic target KCMF1 to prevent cancer development and its growth in RCC. Networking of KCMF1 with RAD6 at C-terminal and UBR4 at N-terminal composited a N-recognins E2-E3 complex that targets the destabilized and misfolding proteins for lysosome-mediated degradation and autophagy [18]. Interestingly, we observed discrepancy in construction and colocalization of RAD6-KCMF1-UBR4 protein domains which caused defective and/or structural deformation of ubiquitin ligase (E2-E3) in RCC. However, non-tumor cells maintained the integrity and co-localization of domains intact. In this maiden study, we explored the KCMF1 and its associated proteins along with autophagy and ion channel markers in RCC patients. Experimental evidences from Kwon et. al. first time reported that the N-recognin KCMF1 induce K63-linked ubiquitination followed by K27-linked ubiquitination by the non-canonical N-recognin UBR4 of target proteins under oxidative stress and/or chronic hypoxic condition [22]. Persisted hypoxia considered as major factor for the development and progression of RCC. 80% of RCC cases possess inactivation and/or genetic mutation in vHL E3 ligase which directs the ubiquitylation of HIF1A and promotes its degradation by UPS (ubiquitination proteasome system) [23][24]. HIF1A is well known for O_2 sensing and maintains stress level under hypoxic condition [25]. But in RCC, defective vHL stabilized HIF1A which migrates to the nucleus and promote the transcription of VEGF and other angiogenesis promoting factors [20]. On the basis of these previous documentations, we further investigated the level of HIF1A in tumor tissue biopsy of same patients in which we examined KCMF1 through confocal microscopy. We observed higher localization of HIF1A in the nucleus of tumor cells whereas nucleus as well cytosolic localization of HIF1A is absent in non-tumor tissue. Inadequate synthesis and fusion of RAD6-KCMF1-UBR4 might be responsible for accumulation of HIF1A in tumor tissue. Till date the interaction and mechanism of HIF1A degradation via N-recognin KCMF1 E3 ligase remains unexplored in all cancer types.

KCMF1-designed E2-E3 ligase have RING domain which targets the unidentified N-end rule substrate for lysosomes-mediated degradation and autophagy [26][18]. Therefore, we determined the autophagy markers LC3B and p62 in tumor samples both at m-RNA and protein level. In this study, we found that the both autophagome marker, LC3B and N-recognin, p62, substrate degradation markers were down regulated in tumor tissue sample in contrast to non-tumor tissue. While PBMCs shows different trend of p62 at m-RNA level. Recently, Kwon et al. suggested that ZZ domains of KCMF1 retain sequence similarity with the UBR box of UBR1 and the ZZ domain of the autophagic N-recognin p62, which further directed the targeted substrate to macroautophagy

instead of UPS for degradation [22]. These finding further strengthen our hypothesis that the deficiency of p62 and KCMF1-UBR4 proteins abolished ubiquitin ligase function and autophagy in tumor cells. Reduced autophagosome and ubiquitin ligase led to the aggregation of misfolding proteins and defective organelles, resulting in acquiring of misbehaviour towards our own system.

Originally KCMF1 was identified through differential screen in *A. californica* [27]. Till date, the functional and structural evidences of KCMF1 are not defined that link to potassium channel signalling. But still in this paper we are trying to understand the possible link between KCMF1 with ions and its channels. KCMF1 is a zinc finger protein whose ZZ domain required two zinc ions at their enzymatic active site for ligand binding and protein scaffolding [28]. Therefore proper concentration and optimum location of zinc ions are necessary for their function. Thus, we determined the level of ions such as zinc, potassium and sodium through ICP-MS in tumor and non-tumor cells. Interestingly we obtained approximately 2-fold reduction of Zn in tumor cells which clearly justified the functional deficiency of KCMF1 in RCC cancer cells. Simultaneously, we recorded a significantly higher level of sodium and potassium in tumor cells. Hence, hyperkalaemia (high potassium) tumor microenviourment were created through ion flux as well as from dying tumor cells which limit the function of effector cells [29]. Additionally, altered expression of potassium ions channels (KV1.3 and KCNN4) was observed in tumor tissue which are essential for maintenance of ions flux inside and outside the cells, since early development of kidney and its branching morphogenesis are dependent upon KCMF1 [30].

In the present study first we analyzed the overall aspects of KCMF1 in tumor condition and simultaneously monitored the function of KCMF1 in PBMCs and tissue associated memory T cells to expand the lifespan of immunotherapy. Therefore we determined the function of KCMF1 in both RCC tumor tissue and PBMCs infiltrated memory T cells.

Chapter -2

KCMF1 linked ubiquitin ligase mediated autophagy regulation in CD8^{+} memory T cells of RCC patient

4.1 Reduction in prevalence of activated $CD8^+$ memory T cells subsets in PBMCs of RCC patients.

To our knowledge, this is the first study to report the frequency of $CD8^+$ memory T cell subsets in PBMCs of patients with RCC. By gating $CD4^+$ and $CD8^+$ T cells for CD45RA and CCR7 markers, both $CD4^+$ and $CD8^+$ memory T cell subsets including TCM ($CD45RA^-CCR7^+$), TEM ($CD45RA^-CCR7^-$), TEFF ($CD45RA^+CCR7^-$) and naïve T cells ($CD45RA^+CCR7^+$) were identified. The frequency of TCM, TEFF, and naïve $CD8^+$ memory T cells is low in the peripheral blood mononuclear cells (PBMCs) of patients when compared to age-matched controls **Figure 1B(a and b).** The gating strategy for these cells was described in **Figure 1(A)**. Although, there is an increase in TEM cells in patients, the degranulation (CD107a) of each $CD8^+$ memory T cell subset is significantly reduced **Figure 1B(c and d),** indicating that the immune response of these patients may not be adequate. Furthermore, the patients also experienced a substantial decrease in the number of $CD4^+$ memory T cell subsets, except for TCM cells **Figure 1B(f and g).** Moreover, a decreased ratio of $CD4^+/CD8^+$ T cells signifies an immune-compromised state, which may result in tumor growth **Figure 1B(e).** Decreased frequency of these $CD8^+$ memory T cell subsets in RCC, raise doubts about whether they acquire a different phenotype undergo apoptosis. We aimed to elucidate the details of $CD8^+$ memory T cells in RCC and their potential impact on immune function.

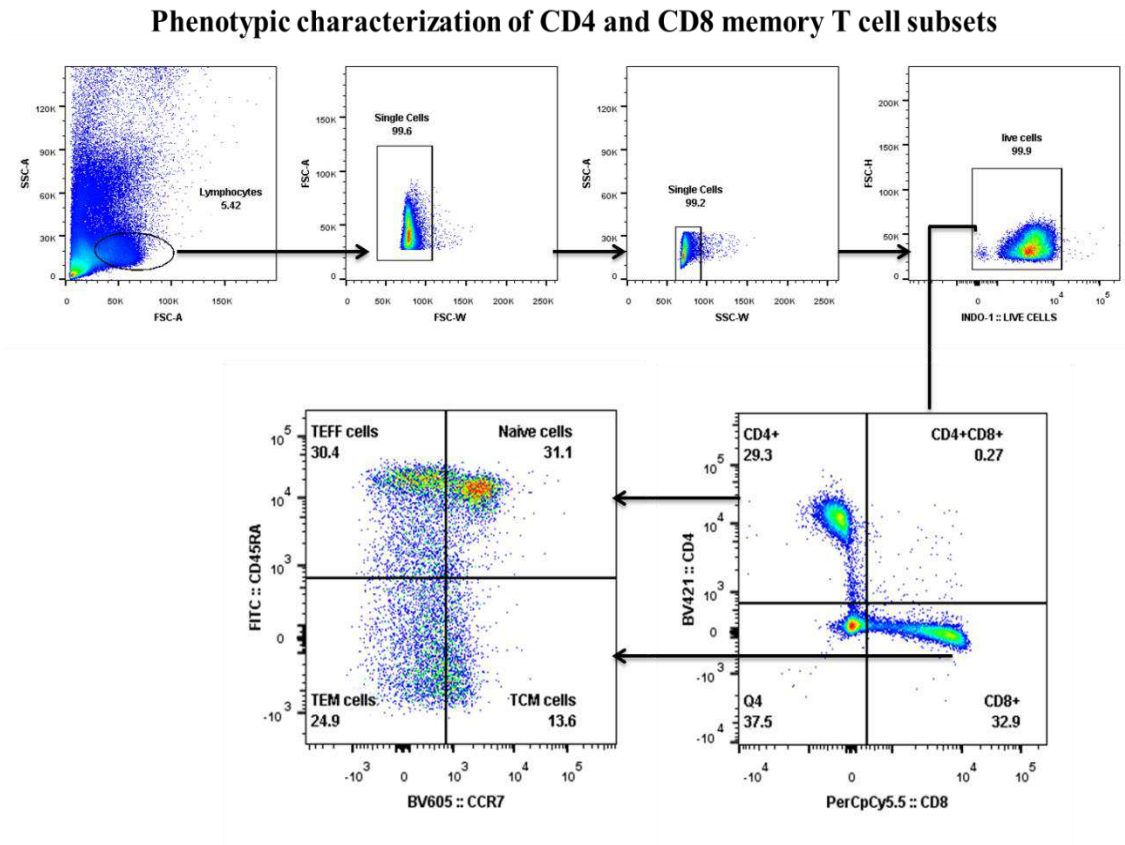

Figure 1(A): Phenotypic characterization of memory T cells subsets: Lymphocytes were gated for Zombie dye to exclude out dead cells from calculation. Live cells were further gated for CD4-

BV421 and CD8-PerCpCy5.5 markers. Both quadrant of $CD4^+$ and $CD8^+$ T cells identified memory T cells subsets including TCM (T central memory;; $CCR7^+CD45RA^-$), TEM (T effector memory;; $CCR7^-CD45RA^-$), TEFF (Effector T cells ;; $CCR7^-CD45RA^+$) and Naïve T cells ($CCR7^+CD45RA^+$). Each subset of memory T cells was further used to determined degarularity and regulatory nature of cells on the basis of CD107a and $FOXP3^+CD25^+$ respectively. Graphical representation of each subset including activation and regulatory markers in patient and control was shown below.

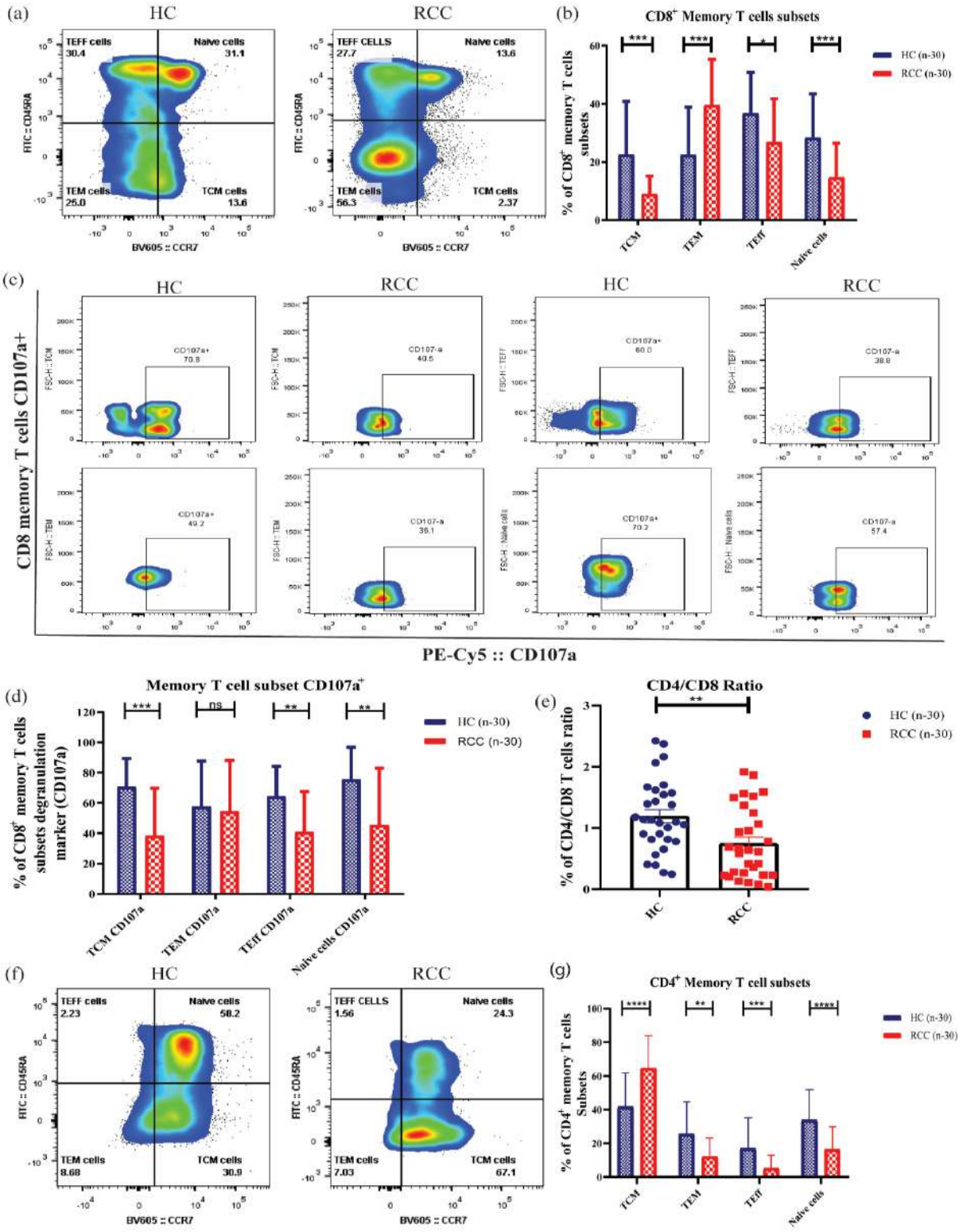

Figure-1: phenotypic characterization of memory T cell subsets in circulation of RCC patients: Both CD4+ and CD8+ memory T subsets were identified on the basis of CD45RA versus CCR7 staining. (a) Pseudocolour plot demonstrated the frequency of TCM, TEM, Teff and Naïve T cells in PBMCs of patients and controls. (b) Quantification of CD8+ memory T cell subsets were represented via bar diagram (n-30). (c and d) Gating strategy and frequency of CD107a+ CD8+ memory T cells subsets in case and control, MFI of CD107a+ CD8+ memory T cells subsets were decreased in patients (n-30). (e) Bar graph presented the ratio of CD4+/CD8+ T cells in among study subjects (n-30). Mann-whiteny U test was performed to analyze unpaired non-parametric, single variable dataset. (f and g) Example plot of CD4+ memory T cell subsets in PBMCs. Bonferroni-Dunn post hoc (Two-way ANOVA) test were used for unpaired non-parametric multiple comparisons of memory T cell subsets including CD107a+, between patients and controls (b, d and g). Here, cell type are considered as group whereas, patients and controls are used as two independent variable (b, d and g). All the data was presented in Mean±SD format. **p<0.01, ***p<0.001, ****p<0.0001.

4.2 $CD8^+$ memory T cells subsets possessed regulatory phenotype in circulation of RCC.

In our preliminary findings, we observed a surge in the fraction of $CD4^+$ TCM and $CD8^+$ TEM cells in RCC patients; however, the nature of these cells still needs to be determined. Accordingly, we further examined the regulatory phenotype of $CD8^+$ memory T cell subsets, focusing specifically on the $FOXP3^+CD25^+$ markers. Total percentage of $FOXP3^+CD25^+$ dual positive regulatory T cells (both $CD4^+$ and $CD8^+$ T cells) tends to be elevated in the PBMCs of patients than in healthy controls **Figure 2(a, b, c and d)**. Moreover, both $CD4^+$ and $CD8^+$ memory T cells subsets, including TCM, TEM, TEFF, and naïve T cells, exhibited a regulatory phenotype ($FOXP3^+CD25^+$) in PBMCs of patients with RCC **Figure 2(e and f).** Bar diagrams show the percentage of regulatory memory T cell subsets **Figure 2(g and h).** The gating strategy for these cells was described in the supplementary file. In addition to Treg cells, both $CD4^+$and $CD8^+$ memory Tcells subsets may play a pivotal role in the pathogenesis and progression of RCC. These findings suggest that the regulation of memory T cell subsets may represent a valuable target for future therapeutic interventions in RCC.

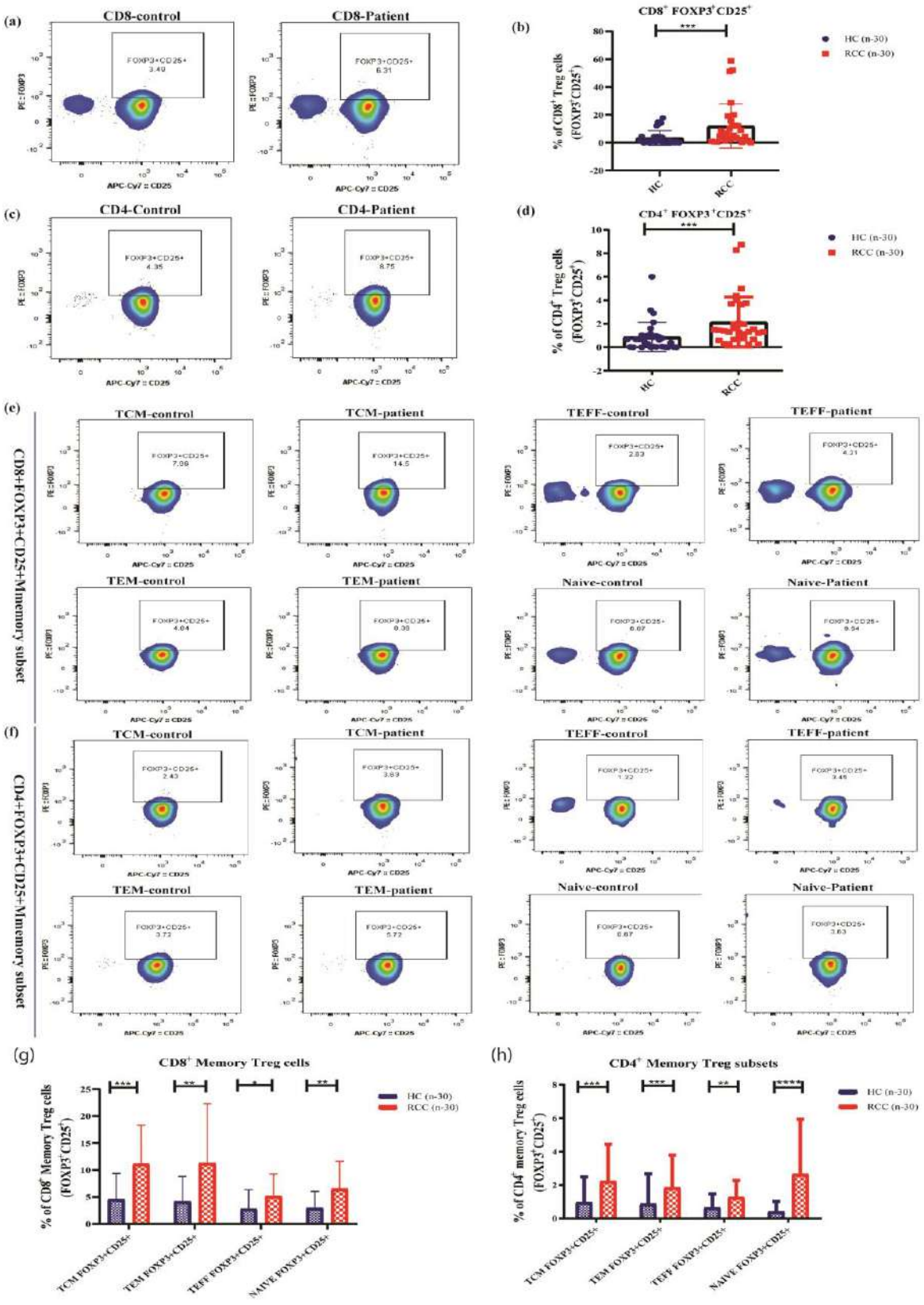

Figure 2: Identification of regulatory CD8+ memory T cells subsets in RCC patients.: (a and b) The Foxp3+CD25+ marker was used to identify regulatory T cells. The frequency of CD8+ and CD4+ Tregs in patient PBMCs was shown in the example figure. (c and d) Bar diagram was used to show the frequency of Treg in the study individuals (n=30). In order to separate regulatory memory T cells in PBMCs, both CD8+ and CD4+ memory T cells are further gated for FOXP3+CD25+. The upper panel of this picture, which depicts CD8+ memory Tregs, and the

lower panel, which depicts CD4+ memory Tregs in the patient and control, are representative diagrams of these cells. (g and h) Prevalence of both CD4+ and CD8+ memory Treg cells within the population of memory T cells were displayed via bar diagram in among cases and controls (n=30). Bonferroni-Dunn post hoc (Two-way ANOVA) test were used for unpaired non-parametric multiple comparisons of regulatory memory T cell subsets between patients and controls (g and h). Mann-whiteny U test was performed to analyze unpaired non-parametric, single variable dataset (b.d). All the data was presented in Mean±SD format. **p<0.01, ***p<0.001, ****p<0.0001.

4.3 Deformity in construction of RAD6-KCMF1-UBR4 (E2-E3) ubiquitin ligase in $CD8^+$ memory T cells of RCC patients.

Notably, we have found a deficiency and the regulatory nature of $CD8^+$ memory T cells in RCC. However, until now, the cause of dysfunctionality and/or apoptosis of $CD8^+$ memory T cells in RCC remain unclear. Immunologically, autophagy is considered a critical phenomenon regulating the long–term survival and effector function of memory T cells to combat disease [31]. To understand this phenomenon, we studied the newly identified ubiquitin ligase called RAD6-KCMF1-UBR4 and its mediated autophagy in sorted $CD8^+$ memory T cells. It has been previously shown that miRNA 210 binds with the 3'UTR of KCMF1, promoting its degradation in preeclampsia [32]. However, in RCC, studies have shown that the expression of miRNA 210 is upregulated in tumor tissue, leading to promotion of tumor growth and disease recurrence [33][34]. In the immune cells, the induction of miRNA 210 is triggered by the activation of immune cells [35][36]. Intriguingly, our research has revealed reduced levels of miRNA 210 in $CD8^+$ memory T cells isolated from PBMCs and tumor tissues in patients as presented in **Figure 3(a).** Furthermore, approximately 2-fold decline was observed in KCMF1 expression in the $CD8^+$ memory T cells of patients, in contrast to the controls **Figure 3(b).** These findings suggest that there is a dysregulation in the activation and function of KCMF1 in these cells. KCMF1 (E3) primarily mediates lysosomal degradation and autophagy through the formation of E2-E3 ubiquitin ligase, which interacts with RAD6 (E2) at the C-terminal and UBR4 (E2) at the N-terminal. Particularly, the ligase and autophagy pathways are crucial for the maintenance of $CD8^+$ memory T-cell function and turnover. Therefore, we further investigated the complex interactions involving E2-E3 ubiquitin ligase and autophagy in the context of KCMF1. The protein levels of KCMF1 and RAD6 were downregulated, while UBR4 was increased in $CD8^+$ memory T cells of the patients, as demonstrated in **Figure 3(c,d and e)**. Moreover, Pearson's correlation coefficient for colocalization of RAD6-KCMF1 and KCMF1-UBR4 domains was significantly reduced in the patient's $CD8^+$ memory T cells. However, upon closer inspection of confocal images, the colocalization of RAD6-KCMF1 and KCMF1-UBR4 domains appeared intact (white region) in healthy $CD8^+$ memory T cells as illustrated by **Figure 3(f and g)**. These findings suggest that the

construction and integration of E2-E3 ligase in $CD8^{+}$ memory T cells is disrupted in patients.

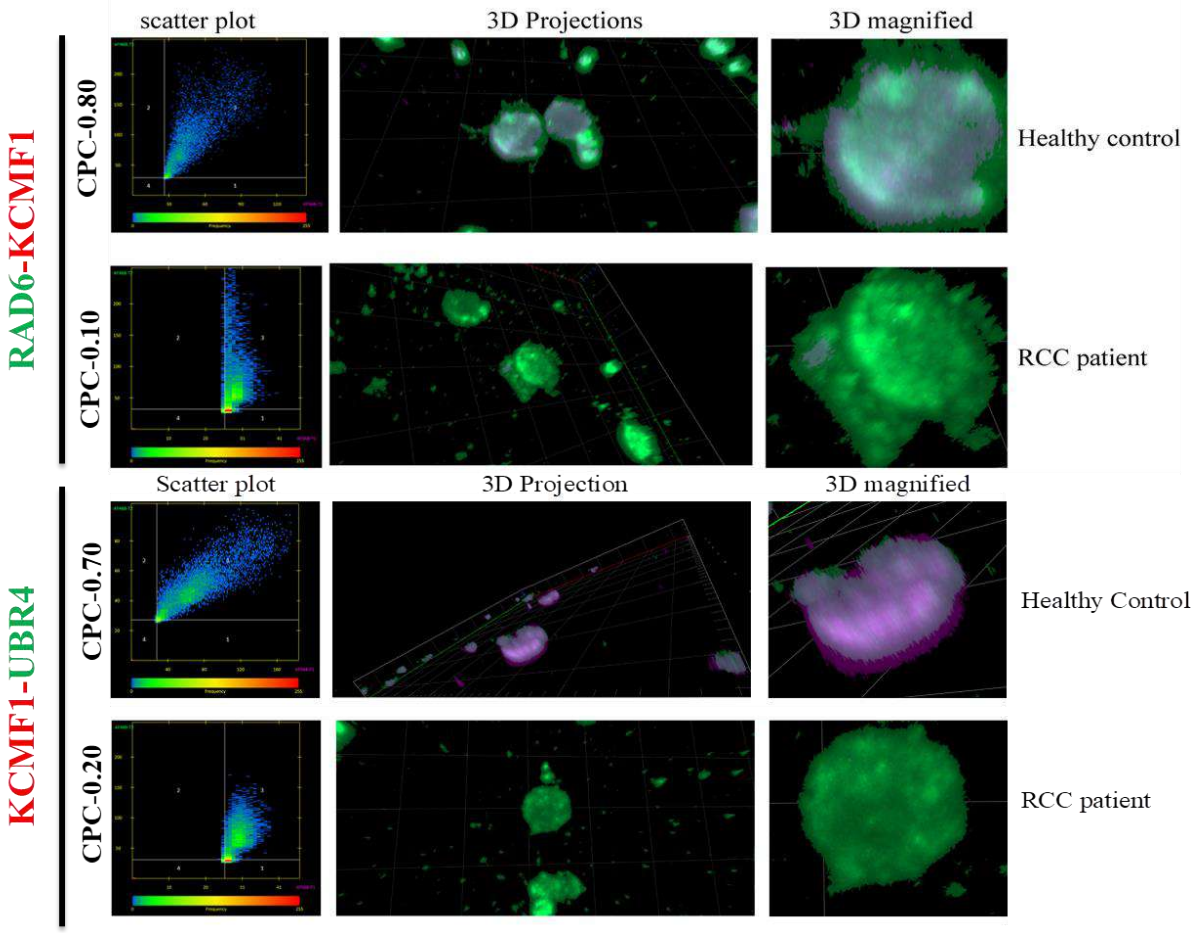

Figure 2: Recognition of E2-E3 ligase complex in sorted memory T cells: RAD6 and UBR4 were co-localized with KCMF1 in age matched control memory T cells whereas KCMF1 and its associated proteins were lost in patients. Scatter plot shown increase intensity of the pixel co-localization of protein domain in control as compared to patients. Indeed in magnified image white coloured represent the region where domains are submerged into each other. *CPC-Correlation Person's coefficient**.**

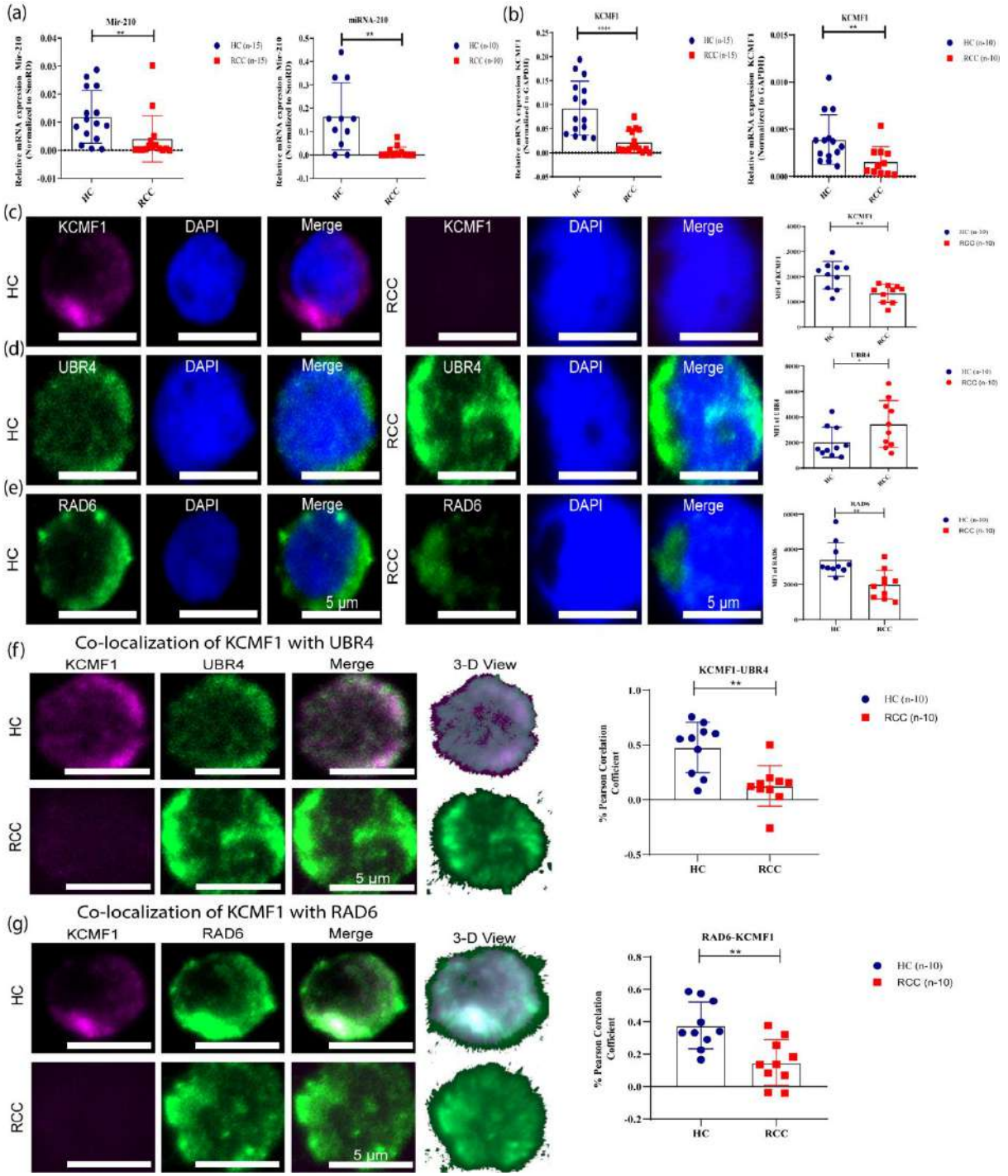

Figure-3. Quantification of KCMF1 associated ubiquitin ligase in CD8+ memory T cells. (a and b) Relative mRNA expression of miRNA 210 and KCMF1 were decreased in CD8+ memory T cells from PBMCs and tumor tissues of RCC patients (blood; n-15, tissue; n-10). (c and e) Protein expression of KCMF1, RAD6 and UBR4 in CD8+ memory T cells were detected through confocal microscopy at 100X. Here, upper panel spectacle the individual expression of KCMF1 and its associated domains. (f and g) In lower panel the colocalization of KCMF1-UBR4 and KCMF1-RAD6 domains were demonstrated in patient and control. Pearson correlation coefficient (PC) was used to quantify the co-localization of KCMF1 with RAD6 and UBR4. Co-localization of KCMF1-RAD6 and KCMF1-UBR4 were significantly reduces in CD8+ memory T cells of among patients (n-10). MFI of KCMF1, RAD6 and UBR4 had shown adjacent of the

representative micrographs (n-10). Scale bar (5um) are shown in images. Data was presented in Mean ± SD format. Mann Whitney U test was used to evaluate the significance of unpaired non-parametric, single variable dataset obtained from patients and controls. **p < 0.01, ***p < 0.001, ****p < 0.0001.

4.4 Abatement in autophagy alters mitochondria polarization in $CD8^+$ memory T cells of patients.

Defects in ubiquitin ligase formation can lead to impaired autophagy and a disruption in downstream functions of $CD8^+$ memory T cells. We analyzed the levels of LC3B, a marker of autophagosome, and P62, a substrate of N-recognin degradation, in sorted $CD8^+$ memory T cells. Notably, both mRNA and protein expression of LC3B and P62, that play a critical role in the autophagic process, essential for cellular homeostasis and immune function, significantly declined, as shown in **Figure 4(a, b, c and d).** Furthermore, recent studies have suggested that P62 is involved in cytoprotection by salvaging mitochondria and preventing cellular apoptosis. Kwon et al. revealed that P62 plays a critical role in this cytoprotective pathway via the degradation of destabilized proteins through autophagy. Moreover, the generation and survival of $CD8^+$ memory T cells is reportedly dependent on autophagy. Research indicates that any alteration to this pathway may result in mitochondrial defects and subsequent apoptosis, or programmed cell death. To assess this, JC.1 was used to measure the mitochondrial polarization in $CD8^+$ memory T cells. A noticeable decrease in the red/green ratio of the JC.1 dye was observed, as demonstrated in **Figure 4(e),** suggesting a depolarized mitochondrial membrane in the patients. Correspondingly, we examined the level of apoptosis using Annexin/PI kit**.** Our study showed a significant increase in early and late apoptosis, as well as some necrosis of $CD8^+$ memory T cells in patients **Figure 4(f)**. Experimental evidence supported our hypothesis that a shortage of E2-E3 ubiquitin ligase results in autophagy defect, which alters mitochondrial depolarization, resulting in apoptosis of these cells. These findings elucidate the underlying mechanisms responsible for the decline of $CD8^+$ memory T cells in patients.

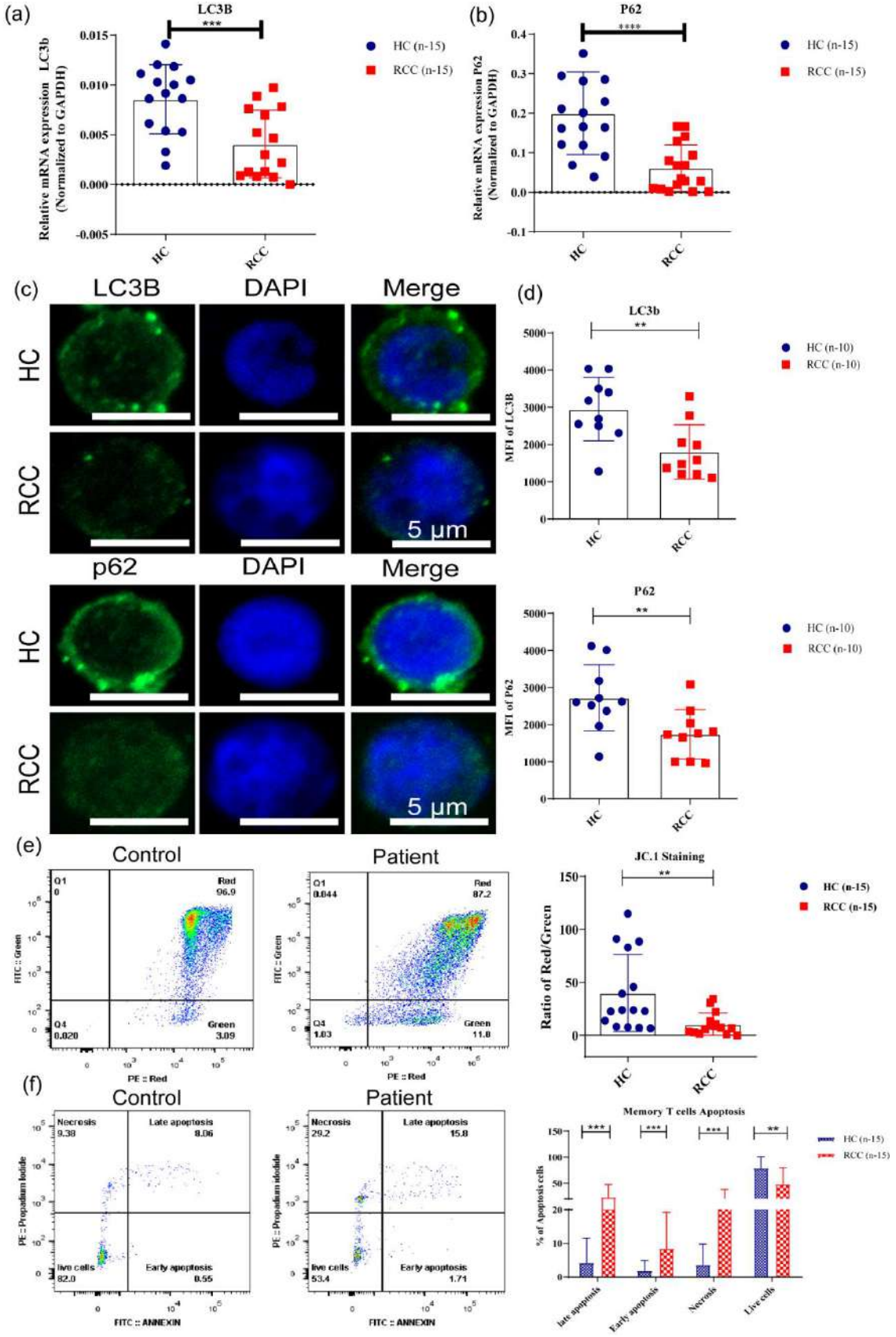

Figure-4. Evaluation of autophagy marker, mitochondria depolarization and apoptosis in CD8+ memory T cells from PBMCs. (a and b) Relative mRNA expression of LC3B and p62 were decreased in CD8 memory T cells of patients (n-15). (c) Confocal images displayed basal level of LC3B and P62 expression in CD8+ memory T cells of control and RCC patient. (d) Bar diagram

demonstrated the significant difference in protein expression of LC3B and p62 in among study subjects (n-10). (e) Pseudocolour plot express red (PE) and green (FITC) signal of JC.1 dye. Decreased ratio of Red/green signal indicates increased depolarization of CD8+ memory T cells in patients (n-15) which shown by adjacent bar diagram. (f) Characterization and frequency of apoptotic CD8+ memory T cells in among study subjects (n-15). All data are analyzed and represented as Mean ± SD. Scale bar (5um) are shown in left corner of the images. Mann Whitney U test was used to evaluate the significance of unpaired non-parametric, single variable dataset obtained from patients and controls (a, b, d and e). Bonferroni-Dunn post hoc (Two-way ANOVA) test were used for unpaired non-parametric multiple comparisons of apoptotic stages of memory T cell between patients and controls **$p < 0.01$, ***$p < 0.001$, ****$p < 0.0001$.

Autophagy defects in tissue resident $CD8^+$ memory T cells (TRMs) of RCC patients.

The regulation of autophagy determines the tumor immunity [37]. Therefore, we analyzed the expression of autophagy markers in the sorted $CD8^+$ memory T cells from both tumor and adjacent non-tumor tissue of patients with RCC. Likewise, mRNA expression of LC3B and p62 in sorted $CD8^+$ memory T cells from tumor tissues was observed similar to the blood infiltrating memory T cells from patients demonstrated in **Figure 5(a and b).** We investigated the infiltration of $CD103^+$ TRMs in both tumor and non-tumor tissues in patients using confocal microscopy, which was expectedly significantly reduced in tumor tissues as compared to non-tumor tissue displayed in **Figure 5(c).** Additionally, we investigated the levels of autophagy markers within TRMs. The punctate formation of LC3B and p62, overlayed with $CD103^+$ T cells, were markedly reduced in tumor tissue compared to non-tumor tissue **Figure 5(d and e).** This suggests that there is diminished and/or abrogated expression of ubiquitin ligase and autophagy markers in the tumor microenvironment. This provides evidence that the distortion and/or structural deviation of ubiquitin ligase limits the formation of autophagosome and N-recognin p62, thereby mediating the degradation of destabilized proteins. Consequently, $CD8^+$ memory T cells lose their cytoprotective properties and undergo apoptosis. This phenomenon was observed both in the blood and tumor tissue infiltrating $CD8^+$ memory T cells of patients with RCC.

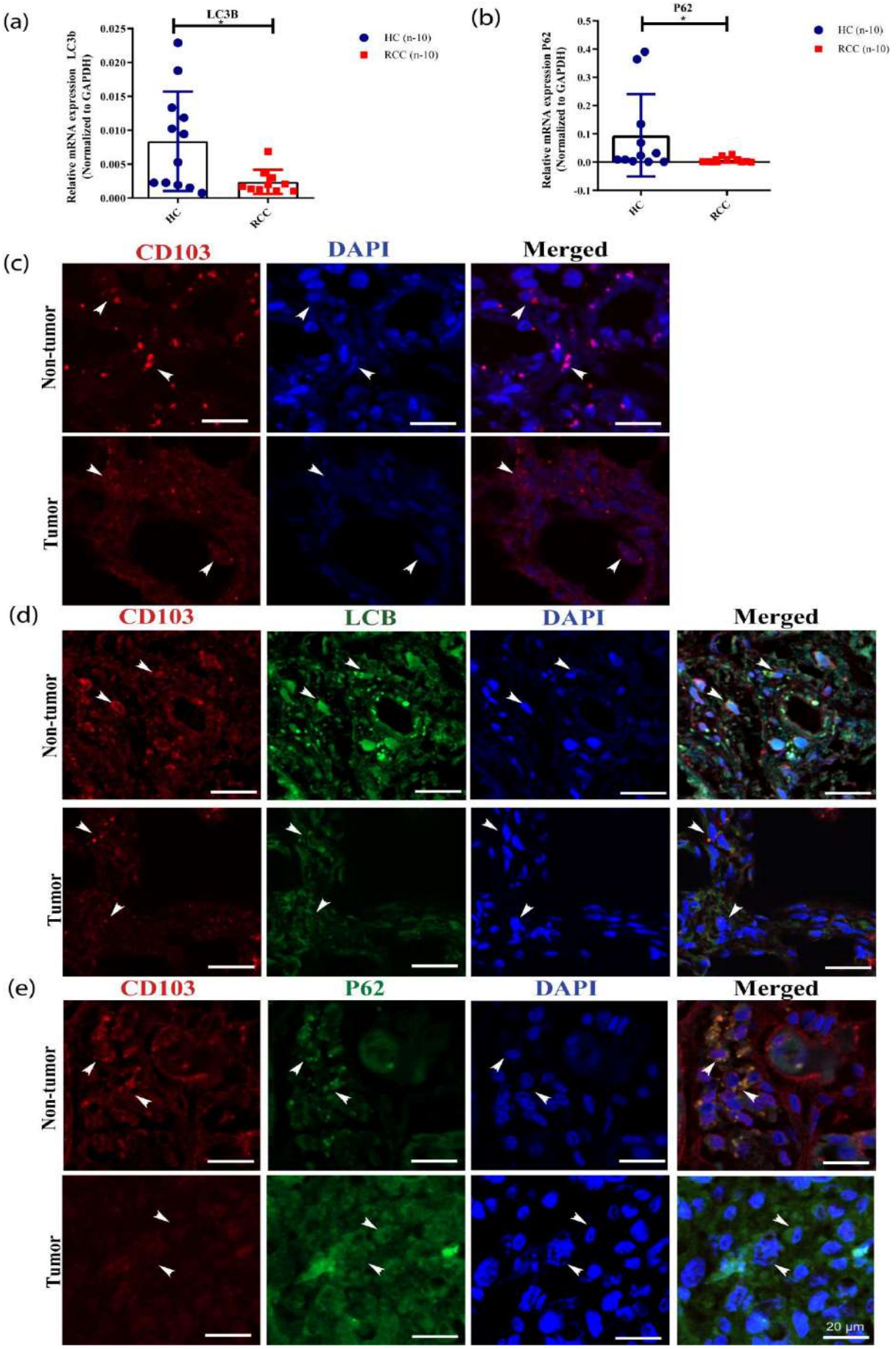

Figure-5. Recognition of autophagy markers in Tissue resident CD8 memory T cells (TRMs). (a and b) Bar graph demonstrated the relative mRNA expression of LC3B and P62, which was found to be reducing in tumor tissues sorted CD8+ memory T cells (n-10). (c) In upper panel, red

punctate indicates the expression of CD103^{+} TRMs in non-tumor tissue whereas these signals relatively dim in tumor tissue. (d and e) Green colour punctate in lower panel shows the expression of autophagy markers LC3B and p62 within CD103^{+} TRMs of adjacent non-tumor. However, tumor tissue displayed diffused and/or abolished expression of autophagy markers in TRMs at tumor site of patient. White arrows indicated TRMs positive for autophagy markers (CD103 $^{+}$ LC3B and CD103 $^{+}$ p62). All images were captured in confocal microscopy at 63X under same settings. Scale bar of images is 20um. **p < 0.01, ***p < 0.001, ****p < 0.0001.

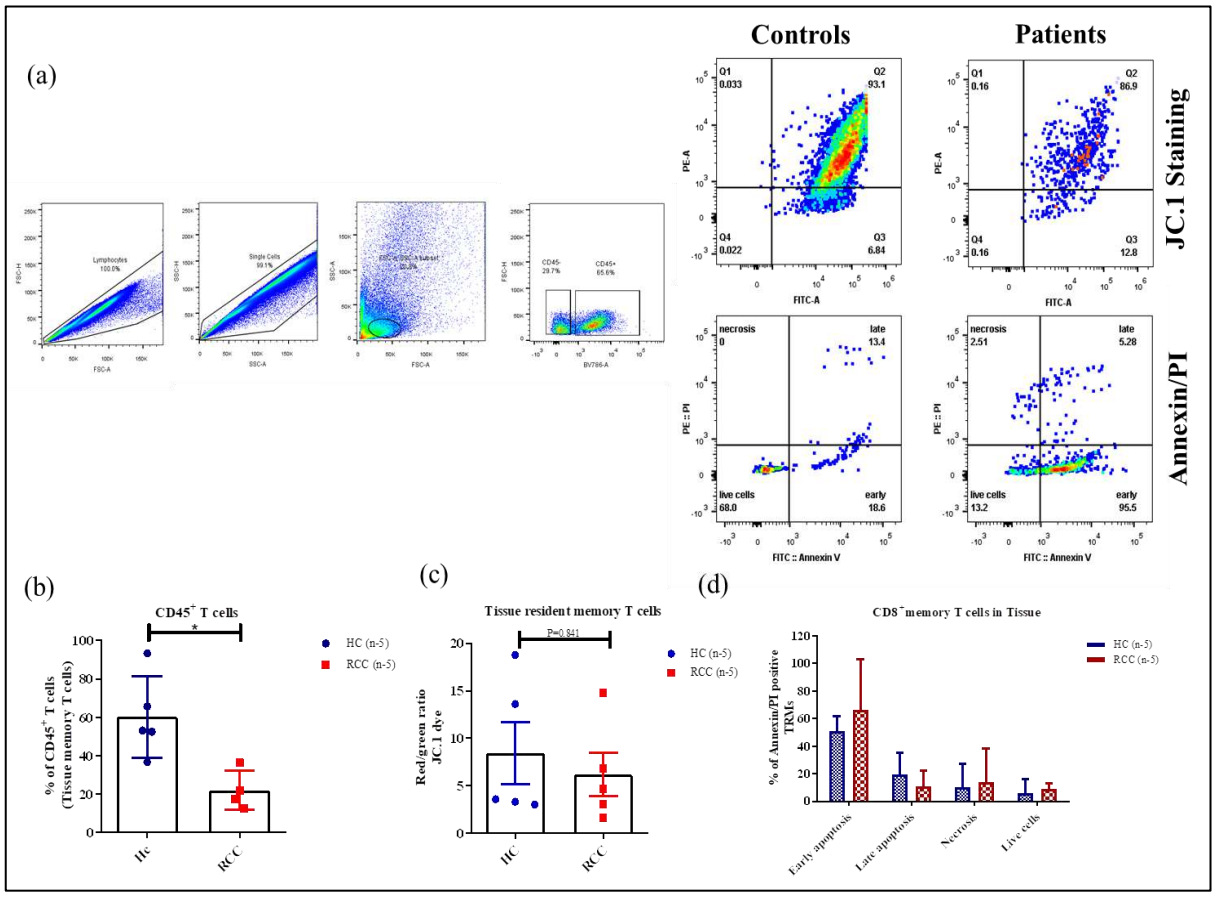

Figure 4: JC.1 and Annexin/PI staining in Tissue resident CD8^{+}memory T cells. (a) Upper panel shown the gating strategy and representative diagram of JC. 1 and Annecin/PI staining in CD8^{+} memory T cells of tumor and adjacent non-tumor tissues of RCC patients. Here, total CD45^{+} T cells were further gated to calculate mitochondrial depolarization and apoptosis of these cells on the basic of red and green filter. **(b)** Bar diagram present the percentage of CD45^{+} memory T cells, which was found to be decreased in tumor tissue. **(c)** This graphs demonstrated the decrease ratio of red/green of JC.1dye indicates the mitochondrial depolarization in tumor tissue of RCC patients. **(d)** Annexin/PI stained shows the different stages of apoptosis in tumor tissue infiltrated CD8^{+} memory T cells in among study subjects. Data was analyzed using Mann-Whitney U test (b and c) and Two way Anova (d). Data is still not significant due to small sample size (n=5), but JC.1 staining clearly shows the trend of mitochondria dysfunction in tumor tissue TRMs. Data was presented in Mean±SD format.

Discussion:

To the best of our knowledge, this is the first study focusing on KCMF1 linked ubiquitin ligase in the regulation of autophagy and apoptosis of memory T cells in RCC patients. Our findings indicate that disruption of E2-E3 complex (RAD6-KCMF1-UBR4) ubiquitin ligase leads to autophagy defect in circulating $CD8^+$ memory T cells and tumor TRMs of patients. Furthermore, the mitochondria become depolarized and memory T cells undergo apoptosis.

RCC has an intricate tumor microenvironment (TME), involved in the angiogenesis, invasion, and metastasis of RCC [38], establishing it as a suitable target for cancer immunotherapy [39]. Furthermore, T cells and myeloid-derived suppressor cells create a distinct immunological environment in RCC [40][41]. Immune checkpoint inhibitor (ICI) therapies like PD-1, PD-L1 and CTLA-4 alone or with vascular endothelial growth factor and tyrosine kinase inhibitors are considered standard therapy in advance RCC patients [8]. However, overall response rate (ORR) of checkpoint inhibitors therapies like PDL1 (nivolumab) alone or with VEGF inhibitor (ipilimumab) was limited to few patients [11][42]. Despite of heavy infiltration of $CD8^+$ T cells in tumors is a perplexing issue in RCC cancer treatment [40]. This is in part can be due to lack of understanding of immune mechanisms undergoing in RCC tumor.

Despite overall $CD8^+$ T cell expansion in tumor tissue, the $CD45RO^+CD8^+$ T cell infiltration declined in RCC [43]. Memory T cells are valuable in providing durable immune response which will keep the tumor progression at bay [44][45]. It can increase the efficiency of immunotherapy. In our study, the frequency of both $CD4^+$ and $CD8^+$ memory T cell subsets were reduced in patients with RCC compared to age-matched controls, excluding $CD4^+$TCM and $CD8^+$ TEM in PBMCs. For the memory T cell subsets including $CD8^+$ effector memory T cells, the release of perforin and granzyme in the TME to kill tumor cells necessitates the degranulation molecule CD107a [46]. We monitored CD107a on memory T cells and since each type of memory T cell has a limited amount of CD107a to release, the cytotoxicity of $CD8^+$ memory T cells was limited in patients. Additionally, we assessed the expression of miRNA 210, considered an activation marker in immune cells. Our results demonstrate a decline in the expression of miRNA210 in the infiltrated memory T cells of patients, suggesting a compromised frequency and function of $CD8^+$ memory T cells in patients with RCC.

In solid cancers, mechanisms such as Fas ligand signalling (melanoma) [47][48], PD1 signalling (hepatocellular carcinoma) [49][50], nutrition and cytokines deprivation and hypoxic conditions trigger activation induced cell death (AICD), programed cell death (PCD) and activated cell autonomous (ACAD)/cytokine withdrawal-induced cell death (CWID) led apoptosis of both effector and memory T cells present in the TME [51]. Memory T cells are resistant to apoptosis in homeostatic conditions, as autophagy pathway contributes to the formation, protection,

maintenance and survival of the memory T cells, regardless of the hostile environment [52][53]. Recently, Kwon et al. identified “KCMF1”, a novel ubiquitin ligase containing a RING domain, interacting with the N-terminal residues of destabilized proteins, to direct them to lysosome mediated degradation and autophagy [18]. The KCMF1 catalytic site contains a zinc finger domain that retains coding similarity with the ZZ domain of UBR1 and the autophagic N-recognin p62, facilitating the targeted substrate to macroautophagy instead of UPS for degradation [22]. This suggests that the disruption of the KCMF1 connected E2-E3 complex impairs autophagy in $CD8^+$ memory T cells. Our study demonstrates that the KCMF1 constitution and its colocalization with RAD6 and UBR4 declined in the circulating $CD8^+$ memory T cells of patients with RCC. However, structural integrity and co-localization of E2-E3 ubiquitin ligase remained intact in $CD8^+$ memory T cells of age matched controls. Corresponding to our hypothesis, autophagosome (LC3B) formation and protein p62 (N-recognin) production was scarce in the patients $CD8^+$ memory T cells. Our findings imply that the absent P62 and KCMF1-UBR4 proteins exterminated the ubiquitin ligase function and autophagy in the patients $CD8^+$ memory T cells.

Acquisition of tissue resident markers, optimization of mitochondrial depolarization and functionality of Tissue resident $CD8^+$ memory T cells (TRMs) are interdependent on autophagy [54][55]. Depending on the cancer type, $CD103^+$TRMs cells can either promote tumor immunosurveillance and/or inhibit tumor growth [56][57]. Nature and prevalence of autophagy in TRMs remains unclear so far in RCC. Consequently, we assessed the markers of autophagy in TRMs through confocal microscopy and observed that the punctate of LC3B and p62 were unapparent in $CD103^+$T cells from tumors of RCC patients. Alternatively, the majority of TRMs in non-tumor tissues were found to be positive for autophagy markers. Defective autophagy may induce depletion of TRMs [54]. Indeed, $CD103^+$T cell infiltration was limited in the tumor tissue of patients with RCC, demonstrating that deficient autophagy limits the survival, function and differentiation of $CD8^+$ memory T cells including TRMs [56]. Our study identified the altered differentiation and functional markers of $CD8^+$ memory T cells from tumor tissues of patients with RCC, for which data is not shown here. Defective autophagy enhances the damaged mitochondria and endoplasmic reticulum congregation [58][59], amplify the reactive oxygen species, and ultimately provoke the apoptosis of T cells in RCC [38]. Correspondingly, we noted the aggregation of depolarized mitochondria along with early and late apoptosis of $CD8^+$ memory T cells in patients with RCC. Besides, we observed poor mitochondrial fitness and cell death of TRMs in the malignant tumor tissue of patients with RCC compared to adjacent non-malignant tissue from the same patients. Among immune cells, memory T cells possess higher mitochondrial mass to sustain a higher spare respiratory capacity, and energy to survive for an extended duration [60]. Additionally, the poor mitochondrial fitness increases the susceptibility of exhaustion and/or death of $CD8^+$ memory T cells [39].

Besides studying the ubiquitin-mediated autophagy mechanism of memory T cells, we also explored the regulatory phenotype of $CD8^+$ memory T cell subsets. Approximately 15–20% of $CD8^+$ memory T cell subsets possessed a regulatory phenotype in patients with RCC, and a higher percentage of both $CD4^+$ and $CD8^+$ Tregs cells were observed in the patient's PBMCs. Moreover, these regulatory cells enhance the immunosurveillance of tumor cells [49], via induced Fas ligand mediated killing of autologous $CD8^+$ T cells [61] and limit the efficacy of anticancer immunotherapy in patients with lung cancer [62]. In vitro expansion and differentiation of memory T cells into effector T cells and autologous transfer may be a better management for disease recurrence. One of the limitations of our study was that the CM (central memory) T cells derived $CD8^+$ effector T cells have a superior expansion potential and defensive capacity than EM derived cells [37]. Our experimental evidence attempts to explain the mechanism of KCMF1 linked ubiquitin ligase and autophagy involved in the dysfunctionality and apoptosis of $CD8^+$ memory T cells in patients with RCC.

Conclusion:

The impairment in the networking and composition of KCMF1 associated ubiquitin ligase resulted in a deficiency in autophagosome formation and altered mitochondria and/or mitochondrial fitness. This led to apoptosis of CD8+ memory T cells in patients with renal cell carcinoma.

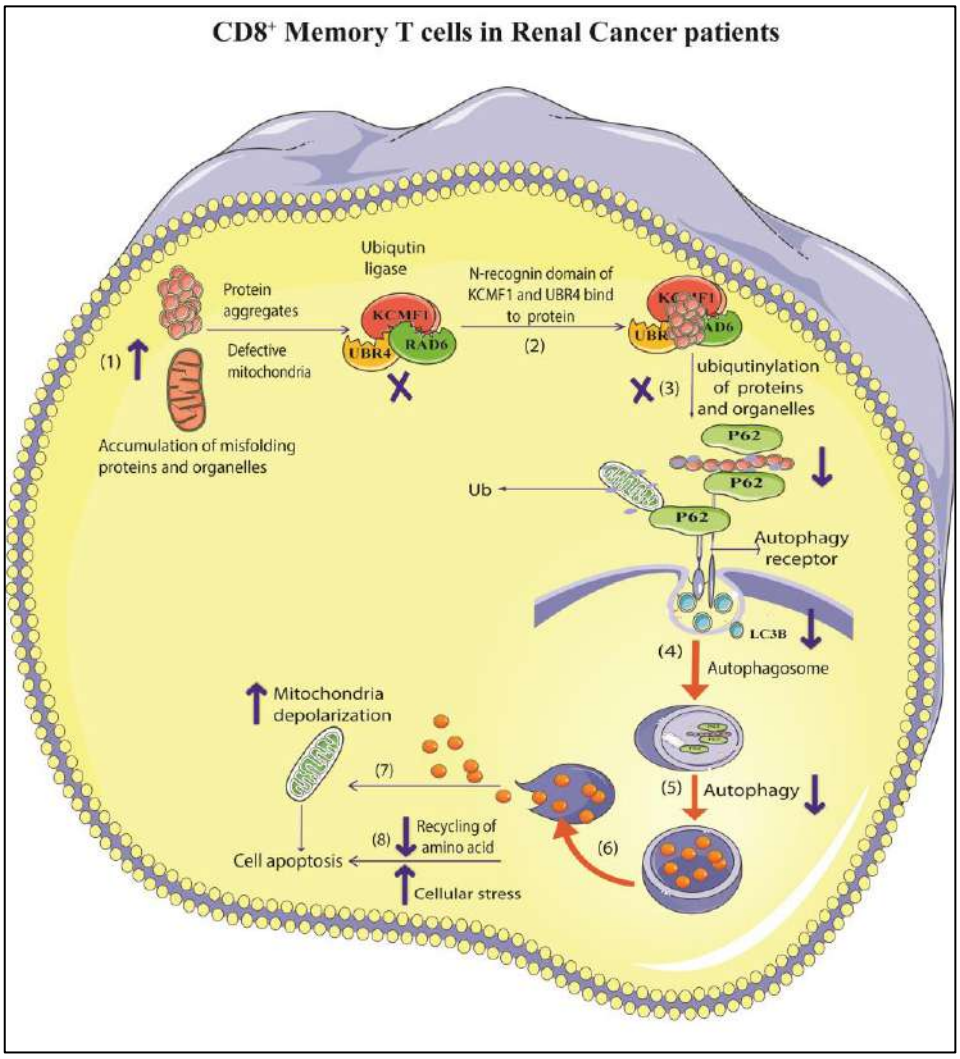

Refrence:

[1] H. Sung *et al.*, "Global Cancer Statistics 2020: GLOBOCAN Estimates of Incidence and Mortality Worldwide for 36 Cancers in 185 Countries," *CA. Cancer J. Clin.*, vol. 71, no. 3, pp. 209–249, May 2021.

[2] S. M. Esagian, I. A. Ziogas, D. Kosmidis, M. D. Hossain, N. M. Tannir, and P. Msaouel, "Long-Term Survival Outcomes of Cytoreductive Nephrectomy Combined with Targeted Therapy for Metastatic Renal Cell Carcinoma: A Systematic Review and Individual Patient Data Meta-Analysis," *Cancers (Basel).*, vol. 13, no. 4, pp. 1–20, Feb. 2021.

[3] A. Méjean *et al.*, "Sunitinib Alone or after Nephrectomy in Metastatic Renal-Cell Carcinoma," *N. Engl. J. Med.*, vol. 379, no. 5, pp. 417–427, Aug. 2018.

[4] U. Swami, R. H. Nussenzveig, B. Haaland, and N. Agarwal, "Revisiting AJCC TNM staging for renal cell carcinoma: quest for improvement," *Ann. Transl. Med.*, vol. 7, no. Suppl 1, pp. S18–S18, Mar. 2019.

[5] U. Capitanio and F. Montorsi, "Renal cancer," *Lancet*, vol. 387, no. 10021, pp. 894–906,

Feb. 2016.

[6] G. P. Abraham, T. Cherian, P. Mahadevan, T. S. Avinash, D. George, and E. Manuel, "Detailed study of survival of patients with renal cell carcinoma in India," *Indian J. Cancer*, vol. 53, no. 4, pp. 572–574, Oct. 2016.

[7] L. Qu *et al.*, "Exosome-Transmitted lncARSR Promotes Sunitinib Resistance in Renal Cancer by Acting as a Competing Endogenous RNA," *Cancer Cell*, vol. 29, no. 5, pp. 653–668, May 2016.

[8] B. I. Rini, S. C. Campbell, and B. Escudier, "Renal cell carcinoma," *Lancet*, vol. 373, no. 9669, pp. 1119–1132, Mar. 2009.

[9] M. C. Ornstein *et al.*, "Individualised axitinib regimen for patients with metastatic renal cell carcinoma after treatment with checkpoint inhibitors: a multicentre, single-arm, phase 2 study," *Lancet Oncol.*, vol. 20, no. 10, pp. 1386–1394, Oct. 2019.

[10] V. Noronha *et al.*, "A real-world data of Immune checkpoint inhibitors in solid tumors from India.," *Cancer Med.*, vol. 10, no. 5, pp. 1525–1534, Mar. 2021.

[11] S. M. Yip *et al.*, "Checkpoint inhibitors in patients with metastatic renal cell carcinoma: Results from the International Metastatic Renal Cell Carcinoma Database Consortium," *Cancer*, vol. 124, no. 18, pp. 3677–3683, Sep. 2018.

[12] M. C. Ornstein *et al.*, "A phase II trial of intermittent nivolumab in patients with metastatic renal cell carcinoma (mRCC) who have received prior anti-angiogenic therapy," *J. Immunother. Cancer*, vol. 7, no. 1, May 2019.

[13] Y. Tomita *et al.*, "Nivolumab versus everolimus in advanced renal cell carcinoma: Japanese subgroup 3-year follow-up analysis from the Phase III CheckMate 025 study," *Jpn. J. Clin. Oncol.*, vol. 49, no. 6, pp. 506–514, May 2019.

[14] L. Lefrançois and A. L. Marzo, "The descent of memory T-cell subsets," *Nat. Rev. Immunol. 2006 68*, vol. 6, no. 8, pp. 618–623, Aug. 2006.

[15] J. L. Reading, F. Gálvez-Cancino, C. Swanton, A. Lladser, K. S. Peggs, and S. A. Quezada, "The function and dysfunction of memory CD8+ T cells in tumor immunity," *Immunol. Rev.*, vol. 283, no. 1, pp. 194–212, May 2018.

[16] R. J. Kishton, M. Sukumar, and N. P. Restifo, "Metabolic Regulation of T Cell Longevity and Function in Tumor Immunotherapy," *Cell Metab.*, vol. 26, no. 1, pp. 94–109, Jul. 2017.

[17] N. Chihara *et al.*, "Induction and transcriptional regulation of the co-inhibitory gene module

in T cells," *Nature*, vol. 558, no. 7710, p. 454, Jun. 2018.

[18] J. H. Hong *et al.*, "KCMF1 (potassium channel modulatory factor 1) Links RAD6 to UBR4 (ubiquitin N-recognin domain-containing E3 ligase 4) and Lysosome-Mediated Degradation," *Mol. Cell. Proteomics*, vol. 14, no. 3, pp. 674–685, Mar. 2015.

[19] E. K. Hoffmann and I. H. Lambert, "Ion channels and transporters in the development of drug resistance in cancer cells."

[20] B. Nadia, C. Dominique, C. Alexandre, C. Kevin, and T. Sandra, "Targeting lysosome function causes selective cytotoxicity in VHL-inactivated renal cell carcinomas," *Carcinogenesis*, vol. 41, no. 6, pp. 828–840, Jun. 2020.

[21] S. Beilke, F. Oswald, F. Genze, T. Wirth, G. Adler, and M. Wagner, "The zinc-finger protein KCMF1 is overexpressed during pancreatic cancer development and downregulation of KCMF1 inhibits pancreatic cancer development in mice," *Oncogene*, vol. 29, no. 28, pp. 4058–4067, Jul. 2010.

[22] A. J. Heo *et al.*, "The N-terminal cysteine is a dual sensor of oxygen and oxidative stress," *Proc. Natl. Acad. Sci.*, vol. 118, no. 50, p. e2107993118, Dec. 2021.

[23] X. Liu, G. Zurlo, and Q. Zhang, "The Roles of Cullin-2 E3 Ubiquitin Ligase Complex in Cancer," *Adv. Exp. Med. Biol.*, vol. 1217, pp. 173–186, 2020.

[24] P. G. Corn, "Role of the ubiquitin proteasome system in renal cell carcinoma," *BMC Biochem.*, vol. 8, no. Suppl 1, p. S4, 2007.

[25] N. V. Iyer *et al.*, "Cellular and developmental control of O2 homeostasis by hypoxia-inducible factor 1α," *Genes Dev.*, vol. 12, no. 2, p. 149, Jan. 1998.

[26] D. Ashton-Beaucage, C. Lemieux, C. M. Udell, M. Sahmi, S. Rochette, and M. Therrien, "The Deubiquitinase USP47 Stabilizes MAPK by Counteracting the Function of the N-end Rule ligase POE/UBR4 in Drosophila," *PLOS Biol.*, vol. 14, no. 8, p. e1002539, Aug. 2016.

[27] S. Beilke, F. Oswald, F. Genze, T. Wirth, G. Adler, and M. Wagner, "The zinc-finger protein KCMF1 is overexpressed during pancreatic cancer development and downregulation of KCMF1 inhibits pancreatic cancer development in mice," *Oncogene*, vol. 29, no. 28, pp. 4058–4067, Jul. 2010.

[28] "KCMF1 (potassium channel modulatory factor 1)." [Online]. Available: http://atlasgeneticsoncology.org/Genes/GC_KCMF1.html. [Accessed: 04-May-2019].

[29] S. K. Vodnala *et al.*, "T cell stemness and dysfunction in tumors are triggered by a common

mechanism," *Science (80-.).*, vol. 363, no. 6434, Mar. 2019.

[30] Z. Li, R. O. Stuart, S. A. Eraly, G. Gittes, D. R. Beier, and S. K. Nigam, "Debt91, a putative zinc finger protein differentially expressed during epithelial morphogenesis," *Biochem. Biophys. Res. Commun.*, vol. 306, no. 3, pp. 623–628, Jul. 2003.

[31] X. Xu *et al.*, "Autophagy is essential for effector CD8 + T cell survival and memory formation," *Nat. Immunol.*, vol. 15, no. 12, pp. 1152–1161, Nov. 2014.

[32] R. Luo *et al.*, "MicroRNA-210 contributes to preeclampsia by downregulating potassium channel modulatory factor 1," *Hypertension*, vol. 64, no. 4, pp. 839–845, 2014.

[33] H. Yoshino *et al.*, "microRNA-210-3p depletion by CRISPR/Cas9 promoted tumorigenesis through revival of TWIST1 in renal cell carcinoma.," *Oncotarget*, vol. 8, no. 13, pp. 20881–20894, Mar. 2017.

[34] X. Wang *et al.*, "Serum exosomal miR-210 as a potential biomarker for clear cell renal cell carcinoma," *J. Cell. Biochem.*, vol. 120, no. 2, pp. 1492–1502, Feb. 2019.

[35] M. Zhao *et al.*, "Up-regulation of microRNA-210 induces immune dysfunction via targeting FOXP3 in CD4(+) T cells of psoriasis vulgaris," *Clin. Immunol.*, vol. 150, no. 1, pp. 22–30, Jan. 2014.

[36] H. Wang, H. Flach, M. Onizawa, L. Wei, M. T. Mcmanus, and A. Weiss, "Negative regulation of Hif1a expression and TH 17 differentiation by the hypoxia-regulated microRNA miR-210," *Nat. Immunol.*, vol. 15, no. 4, pp. 393–401, 2014.

[37] L. DeVorkin *et al.*, "Autophagy Regulation of Metabolism Is Required for CD8+ T Cell Anti-tumor Immunity," *Cell Rep.*, vol. 27, no. 2, pp. 502-513.e5, Apr. 2019.

[38] S. Zhang *et al.*, "Immune infiltration in renal cell carcinoma," *Cancer Sci.*, vol. 110, no. 5, p. 1564, May 2019.

[39] K. Ross and R. J. Jones, "Immune checkpoint inhibitors in renal cell carcinoma," *Clin. Sci. (Lond).*, vol. 131, no. 21, pp. 2627–2642, Nov. 2017.

[40] P. J. Siska *et al.*, "Mitochondrial dysregulation and glycolytic insufficiency functionally impair CD8 T cells infiltrating human renal cell carcinoma," *JCI Insight*, vol. 2, no. 12, Jun. 2017.

[41] Y. G. Najjar *et al.*, "Myeloid derived suppressor cell subset accumulation in renal cell carcinoma parenchyma is associated with intratumoral expression of IL-1β, IL-8, CXCL5 and Mip-1α," *Clin. Cancer Res.*, vol. 23, no. 9, p. 2346, May 2017.

[42] P. Makhov, S. Joshi, P. Ghatalia, A. Kutikov, R. G. Uzzo, and V. M. Kolenko, “Resistance to Systemic Therapies in Clear Cell Renal Cell Carcinoma: Mechanisms and Management Strategies,” *Mol Cancer Ther*, vol. 17, no. 7, 2018.

[43] K. Wu *et al.*, “Accumulation of CD45RO+CD8+ T cells is a diagnostic and prognostic biomarker for clear cell renal cell carcinoma,” *Aging (Albany NY)*, vol. 13, no. 10, p. 14304, May 2021.

[44] N. Principe *et al.*, “Tumor Infiltrating Effector Memory Antigen-Specific CD8+ T Cells Predict Response to Immune Checkpoint Therapy,” *Front. Immunol.*, vol. 11, p. 2907, Nov. 2020.

[45] F. Pagès *et al.*, “Effector Memory T Cells, Early Metastasis, and Survival in Colorectal Cancer,” *N. Engl. J. Med.*, vol. 353, no. 25, pp. 2654–2666, Dec. 2005.

[46] E. Aktas, U. C. Kucuksezer, S. Bilgic, G. Erten, and G. Deniz, “Relationship between CD107a expression and cytotoxic activity,” *Cell. Immunol.*, vol. 254, no. 2, pp. 149–154, 2009.

[47] J. Zhu, P. F. Petit, and B. J. Van den Eynde, “Apoptosis of tumor-infiltrating T lymphocytes: a new immune checkpoint mechanism,” *Cancer Immunol. Immunother. 2018 685*, vol. 68, no. 5, pp. 835–847, Nov. 2018.

[48] J. Zhu *et al.*, “Resistance to cancer immunotherapy mediated by apoptosis of tumor-infiltrating lymphocytes,” *Nat. Commun.*, vol. 8, no. 1, Dec. 2017.

[49] G. Fanelli *et al.*, “PD-L1 signaling on human memory CD4+ T cells induces a regulatory phenotype,” *PLoS Biol.*, vol. 19, no. 4, Apr. 2021.

[50] J. Ma *et al.*, “PD1Hi CD8+ T cells correlate with exhausted signature and poor clinical outcome in hepatocellular carcinoma,” *J. Immunother. cancer*, vol. 7, no. 1, Nov. 2019.

[51] K. Voss, S. E. Larsen, and A. L. Snow, “Metabolic reprogramming and apoptosis sensitivity: defining the contours of a T cell response,” *Cancer Lett.*, vol. 408, p. 190, Nov. 2017.

[52] S. E. Larsen, K. Voss, E. D. Laing, and A. L. Snow, “Differential cytokine withdrawal-induced death sensitivity of effector T cells derived from distinct human CD8+ memory subsets,” *Cell Death Discov.*, vol. 3, no. 1, p. 17031, Dec. 2017.

[53] L. A. Booth, S. Tavallai, H. A. Hamed, N. Cruickshanks, and P. Dent, “The role of cell signalling in the crosstalk between autophagy and apoptosis,” *Cell. Signal.*, vol. 26, no. 3, p. 549, Mar. 2014.

[54] L. Swadling *et al.*, “Human Liver Memory CD8 + T Cells Use Autophagy for Tissue Residence,” *Cell Rep.*, vol. 30, no. 3, pp. 687-698.e6, Jan. 2020.

[55] L. Wang *et al.*, “Autophagy in T-cell differentiation, survival and memory,” *Immunol. Cell Biol.*, vol. 99, no. 4, pp. 351–360, Apr. 2021.

[56] K. Okla, D. L. Farber, and W. Zou, “Tissue-resident memory T cells in tumor immunity and immunotherapy,” *J. Exp. Med.*, vol. 218, no. 4, Apr. 2021.

[57] S. L. Park, T. Gebhardt, and L. K. Mackay, “Tissue-Resident Memory T Cells in Cancer Immunosurveillance,” *Trends Immunol.*, vol. 40, no. 8, pp. 735–747, Aug. 2019.

[58] H. H. Pua, J. Guo, M. Komatsu, and Y.-W. He, “Autophagy Is Essential for Mitochondrial Clearance in Mature T Lymphocytes,” *J. Immunol.*, vol. 182, no. 7, pp. 4046–4055, Apr. 2009.

[59] W. Jia and Y.-W. He, “Temporal Regulation of Intracellular Organelle Homeostasis in T Lymphocytes by Autophagy,” *J. Immunol.*, vol. 186, no. 9, pp. 5313–5322, May 2011.

[60] G. J. W. van der Windt *et al.*, “Mitochondrial respiratory capacity is a critical regulator of CD8+ T cell memory development,” *Immunity*, vol. 36, no. 1, pp. 68–78, Jan. 2012.

[61] L. Strauss, C. Bergmann, and T. L. Whiteside, “Human circulating CD4+CD25highFoxp3+ regulatory T cells kill autologous CD8+ but not CD4+ responder cells by Fas-mediated apoptosis,” *J. Immunol.*, vol. 182, no. 3, pp. 1469–1480, Feb. 2009.

[62] I. Kwiecień *et al.*, “Effector Memory T Cells and CD45RO+ Regulatory T Cells in Metastatic vs. Non-Metastatic Lymph Nodes in Lung Cancer Patients,” *Front. Immunol.*, vol. 13, May 2022.

Impact of the research in the advancement of knowledge or benefit to mankind:

Through high-throughput screening and new state-of-the-art technologies we are able to get deeper insight into immune cell function in tumour microenvironment and identify novel therapeutic targets in cancer. This would be beneficial to furthermore strengthen the existing chemotherapy and/or developed novel therapeutic treatment for large cohort cancer patients. Simultaneously, it will be useful to increase prognosis and overall response rate of immunotherapies for cancer patients, resulting survival of cancer patients will be increased. Afterward of this programme, newly Identified targets and cancer immunotherapy responses will be furthermore validated in clinical sample of large patient's cohort. Moreover this conference build international collaboration for cancer research to identified novel targets for immunotherapy, will aid the private sector organisations in making new immunotherapy pharmacologically which will ultimately help practitioners in treating the patients.